JCB Journal of Cell Biology

ARTICLE

NCAM regulates temporal specification of neural progenitor cells via profilin2 during corticogenesis

Rui Huang[1*], De-Juan Yuan[2,3*], Shao Li[3*], Xue-Song Liang[1], Yue Gao[1], Xiao-Yan Lan[1], Hua-Min Qin[4], Yu-Fang Ma[5], Guang-Yin Xu[2], Melitta Schachner[6,7], Vladimir Sytnyk[8], Johannes Boltze[9], Quan-Hong Ma[2], and Shen Li[1]

The development of cerebral cortex requires spatially and temporally orchestrated proliferation, migration, and differentiation of neural progenitor cells (NPCs). The molecular mechanisms underlying cortical development are, however, not fully understood. The neural cell adhesion molecule (NCAM) has been suggested to play a role in corticogenesis. Here we show that NCAM is dynamically expressed in the developing cortex. NCAM expression in NPCs is highest in the neurogenic period and declines during the gliogenic period. In mice bearing an NPC-specific NCAM deletion, proliferation of NPCs is reduced, and production of cortical neurons is delayed, while formation of cortical glia is advanced. Mechanistically, NCAM enhances actin polymerization in NPCs by interacting with actin-associated protein profilin2. NCAM-dependent regulation of NPCs is blocked by mutations in the profilin2 binding site. Thus, NCAM plays an essential role in NPC proliferation and fate decision during cortical development by regulating profilin2-dependent actin polymerization.

Introduction

The development of the mammalian cerebral cortex requires spatially and temporally orchestrated proliferation, migration, and differentiation of neural progenitor cells (NPCs; Greig et al., 2013). Radial glial cells (RGCs) in the ventricular zone (VZ) contribute to the generation of cortical layers directly or indirectly through intermediate progenitor cells (IPCs; Gal et al., 2006; Haubensak et al., 2004). Cortical neurons are generated in a defined temporal sequence in which neurons in deeper layers are generated first. Following neurogenesis, astrocytes appear shortly before birth, whereas oligodendrocytes emerge postnatally in mammals (Kohwi and Doe, 2013). Both intrinsic and extrinsic factors contribute to this developmental sequence. In humans, disturbance of this highly elaborate process leads to neurodevelopmental defects ranging between devastating malformations and relatively mild abnormalities causing neurological diseases such as epilepsy, schizophrenia, and autism spectrum disorder (Gaspard and Vanderhaeghen, 2011).

The neural cell adhesion molecule (NCAM) is a membrane-bound cell recognition molecule of the immunoglobulin superfamily. NCAM contributes to the nervous system development by influencing neuronal migration, neurite outgrowth, synapse formation, and synaptic plasticity (Sytnyk et al., 2017). Alternative splicing of NCAM transcripts generates three major isoforms: NCAM180, NCAM140, and NCAM120. NCAM180 and NCAM140 are transmembrane isoforms bearing an intracellular domain, which is longer in NCAM180. NCAM120 is anchored to the membrane via a glycosylphosphatidylinositol linkage (Sytnyk et al., 2017). Soluble extracellular NCAM fragments can be produced by NCAM ectodomain shedding (Hübschmann et al., 2005; Secher, 2010). NCAM-knockout mice display an abnormal brain structure as well as learning and behavioral abnormalities (Brandewiede et al., 2014; Bukalo et al., 2004; Stork et al., 1999; Wood et al., 1998). Moreover, single nucleotide polymorphisms in the *NCAM* gene and/or abnormal polysialylation or proteolysis of NCAM protein alter NCAM function in neurodevelopmental, neuropsychiatric, and neurodegenerative disorders in humans (Brennaman and Maness, 2010; Hidese et al., 2017; Purcell et al., 2001; Wang et al., 2012), suggesting a crucial role of NCAM in cortical development.

[1]Neurology Department, Dalian Municipal Central Hospital affiliated with Dalian Medical University, Dalian, China; [2]Jiangsu Key Laboratory of Translational Research and Therapy for Neuro-Psycho-Diseases, Institute of Neuroscience, Soochow University, Suzhou, China; [3]Physiology Department, Dalian Medical University, Dalian, China; [4]Pathology Department, The Second Hospital of Dalian Medical University, Dalian, China; [5]Biochemistry and Molecular Biology Department, Dalian Medical University, Dalian, China; [6]Center for Neuroscience, Shantou University Medical College, Shantou, China; [7]W.M. Keck Center for Collaborative Neuroscience and Department of Cell Biology and Neuroscience, Rutgers University, Piscataway, NJ; [8]School of Biotechnology and Biomolecular Sciences, University of New South Wales, Sydney, Australia; [9]School of Life Sciences, University of Warwick, Coventry, UK.

*Rui Huang, De-Juan Yuan, and Shao Li contributed equally to this paper; Correspondence to Shen Li: listenlishen@hotmail.com; Quanhong Ma: maquanhong@suda.edu.cn.

NCAM plays a role in regulation of neurogenesis. Recombinant soluble NCAM reduces hippocampal NPC proliferation by heterophilic binding to an unknown cell surface receptor (Amoureux et al., 2000; Shin et al., 2002). Soluble NCAM and overexpression of NCAM140 in NPCs promote differentiation of NPCs into the neuronal lineage (Amoureux et al., 2000; Kim and Son, 2006; Kim et al., 2005; Klein et al., 2014), whereas ectopic expression of NCAM140 in RGCs increases cell proliferation in vivo (Boutin et al., 2009). However, it is unknown whether NCAM is an intrinsic modulator of NPC proliferation and differentiation.

Regulation of the cell cycle plays a crucial role in controlling temporal and spatial production of neural cells (Dehay and Kennedy, 2007; Politis et al., 2008). Cell cycle progression is modulated by the actin cytoskeleton, which regulates cell rounding and rigidity for proper positioning and spindle orientation during mitosis (Heng and Koh, 2010; Kunda and Baum, 2009). Actin cytoskeleton reorganization during mitosis is controlled by actin-binding proteins, among which profilins are essential for cytokinesis (Suetsugu et al., 1999). Profilins are a conserved family of small proteins that facilitate the addition of actin monomers to the fast-growing end of actin filaments by accelerating the ADP–ATP nucleotide exchange (Witke, 2004). Among the four profilin subtypes, profilin2 is most expressed in the central nervous system (Di Nardo et al., 2000), where it contributes to maintaining spine density and dendritic complexity (Michaelsen et al., 2010). Profilin2 also stabilizes spine structure, controls presynaptic vesicular exocytosis (Pilo Boyl et al., 2007), and is required for synaptic plasticity (Chakraborty et al., 2014). However, the role of profilins in cortical development is so far unknown.

Results

NCAM is dynamically expressed in NPCs during cortical development

We first examined the NCAM expression profile. NCAM levels, particularly of the NCAM180 and NCAM140 isoforms, steadily increased in the developing mouse cortex (Fig. S1, A–F). To further analyze the expression of NCAM in distinct cell types, coronal cortical sections at different embryonic stages (embryonic day 12 [E12] to postnatal day 0 [P0]) were coimmunostained for NCAM and either Sox2 (NPCs) or Tuj1 (neurons), respectively. NCAM was expressed in both NPCs (Fig. 1 A) and neurons (Fig. 1 B) in the developing cortex. Quantification of NCAM immunofluorescence intensities revealed that NCAM was predominantly expressed by NPCs in the VZ/subventricular zone (SVZ) and by neurons in the intermediate zone (IZ), cortical plate (CP), and marginal zone (MZ) during the early neurogenic period (E12 to E14). Interestingly, NCAM immunofluorescence intensity in VZ/SVZ in relation to that in the total dorsal brain (Fig. 1 C) as well as average NCAM immunofluorescence density in VZ/SVZ (Fig. 1 D) decreased from E16 onward, reaching the lowest level at E18 and P0 (gliogenic period). In contrast, NCAM immunoreactivity did not change in the IZ and MZ, and it even increased in the CP at E18 and P0 compared with E16, indicating that NCAM levels are maintained during these developmental stages in areas enriched in cortical neurons (Fig. 1, A–D; and Fig. S1 H). These results indicate that NCAM is expressed in NPCs in the early neurogenic period, whereas NCAM expression in NPCs declines during the gliogenic period.

NCAM deficiency results in transiently reduced NPC proliferation in the developing cerebral cortex

We next examined the role of NCAM in NPCs by generating NCAM–conditional knockout (cKO) mice via crossing NCAM-floxed mice with Nestin-cre mice to ablate NCAM expression in NPCs. NCAM was not detectable in NPCs (Fig. S1 H) and other brain cell populations (data not shown) in NCAM-cKO mice. We then examined whether the NPC pool was affected by NCAM deficiency. Numbers of $Pax6^+$ RGCs were reduced in the VZ in NCAM-cKO mice at E12 and E14, but not at E16 and E18, compared with control littermates (Fig. 2, A and B). Numbers of $Tbr2^+$ IPCs, which mainly localize in the SVZ, were also decreased in NCAM-cKO mice at E12, but not at E14 and E16 (Fig. 2, E and F). These results indicate that NCAM deficiency leads to transient reduction of NPC numbers during cortical development.

The total number of $BrdU^+$ cells (Fig. 2 C) and the percentage of proliferating $Pax6^+BrdU^+/Pax6^+$ RGCs (Fig. 2 D) were reduced in NCAM-cKO mice compared with control littermates at E12 and E14, but not at E16 and E18, indicating that NCAM regulates RGC proliferation only during earlier developmental stages. Consistently, the numbers of $Ki67^+$ (Fig. 2, G and H) or $PH3^+$ (Fig. 2, I and J) cells, representing cells in the cell cycle or in mitosis, were also decreased in E12 NCAM-cKO mice. This finding suggests that NCAM deficiency results in fewer NPCs in the cell cycle and mitosis at this stage. The decreased proliferation of NCAM-cKO NPCs was not due to enhanced apoptosis, as the numbers of cleaved active $caspase3^+$ NPCs were similar in NCAM-cKO and control littermates at E12, E14, and E16 (Fig. S2).

We also analyzed whether NCAM deficiency affects cell cycle exit and length in the VZ/SVZ. The cell cycle exit index (proportion of $BrdU^+Ki67^-$ cells in $BrdU^+$ cell population) was increased at E14 in the VZ/SVZ of NCAM-cKO mice compared with control littermates (Fig. 2, K and L). S-phase length, estimated by the proportion of $BrdU^+Ki67^+$ cells in the $Ki67^+$ cell population, was not altered at E14 (Fig. 2, K and M). These data indicate that NCAM deficiency results in enhanced cell cycle exit and decreased NPC proliferation, eventually reducing the NPC pool during the early neurogenic period.

NCAM deficiency delays the generation of cortical neurons

Next, we analyzed whether NCAM regulates the generation of layer-specific neurons at different embryonic stages. The numbers of $Tbr1^+$ neurons in layer VI in NCAM-cKO cortices were decreased at E12 and E14, increased at E16, and unaltered at E18 (Fig. 3, A and D). $Ctip2^+$ neuron numbers in layer V in NCAM-cKO mice were decreased at E12 and E14, but unchanged at E16 (Fig. 3, B and E). The numbers of $Cux1^+$ neurons in layers II–IV in NCAM-cKO mice were reduced at E16, E18, and P0, but returned

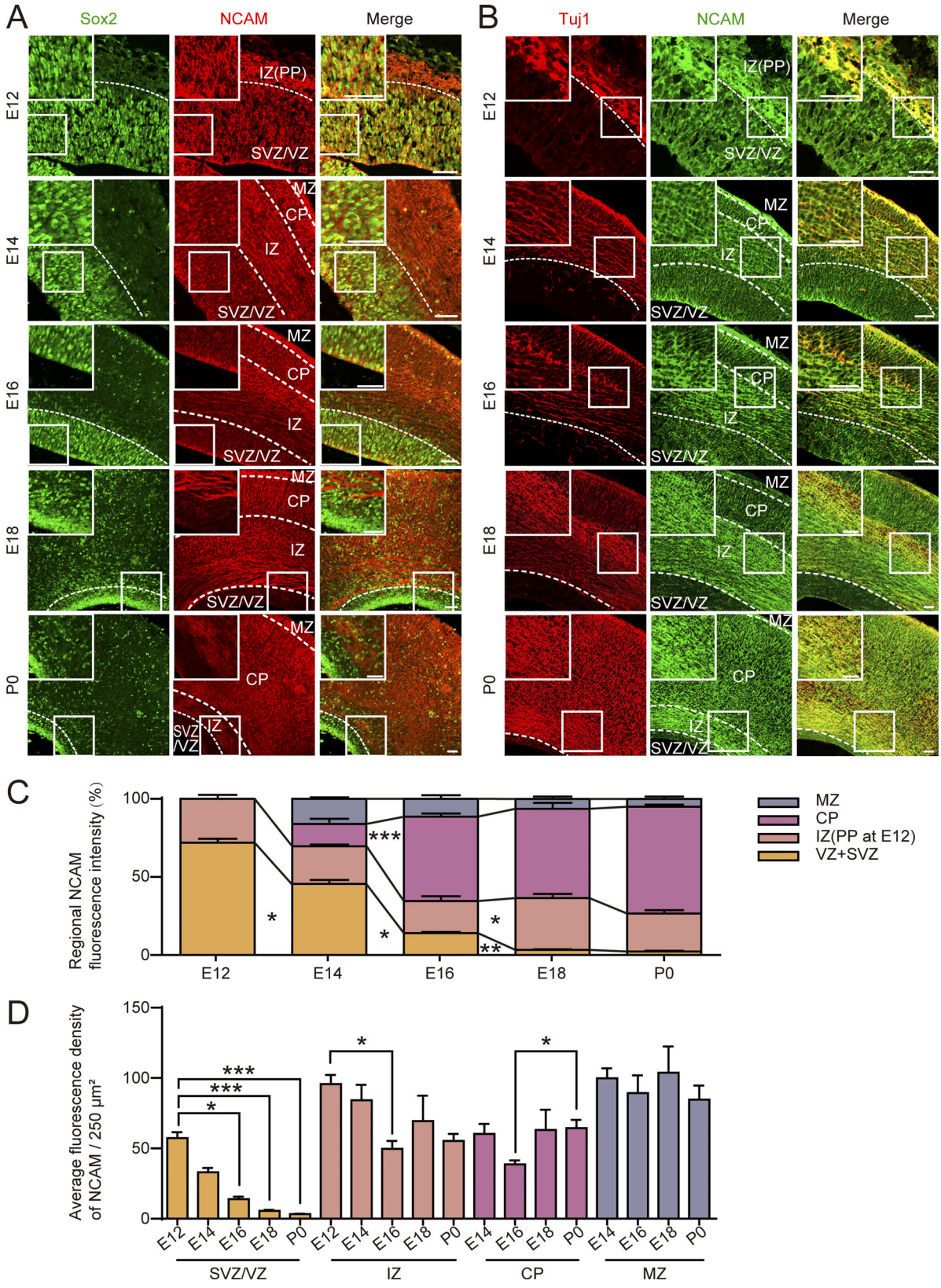

Figure 1. **NCAM is dynamically expressed in NPCs during cortical development. (A and B)** Coronal sections of mouse cortices from indicated embryonic stages were coimmunostained for NCAM and Sox2 (A) or Tuj1 (B). Scale bars, 50 µm. **(C)** Percentages of NCAM$^+$ immunoreactivity in each layer. **(D)** Average immunofluorescence density of NCAM in each layer. $n = 9$ brain slices from three mice. Values represent mean ± SEM. *, $P < 0.05$; **, $P < 0.01$; ***, $P < 0.001$ (two sided). One-way ANOVA with Bonferroni corrections (IZ, CP, and MZ in C and MZ in D), Dunnett's T3 correction (VZ/SVZ in C), and Kruskal-Wallis test with Dunn-Bonferroni correction (VZ/SVZ, IZ, and CP in D). PP, preplate.

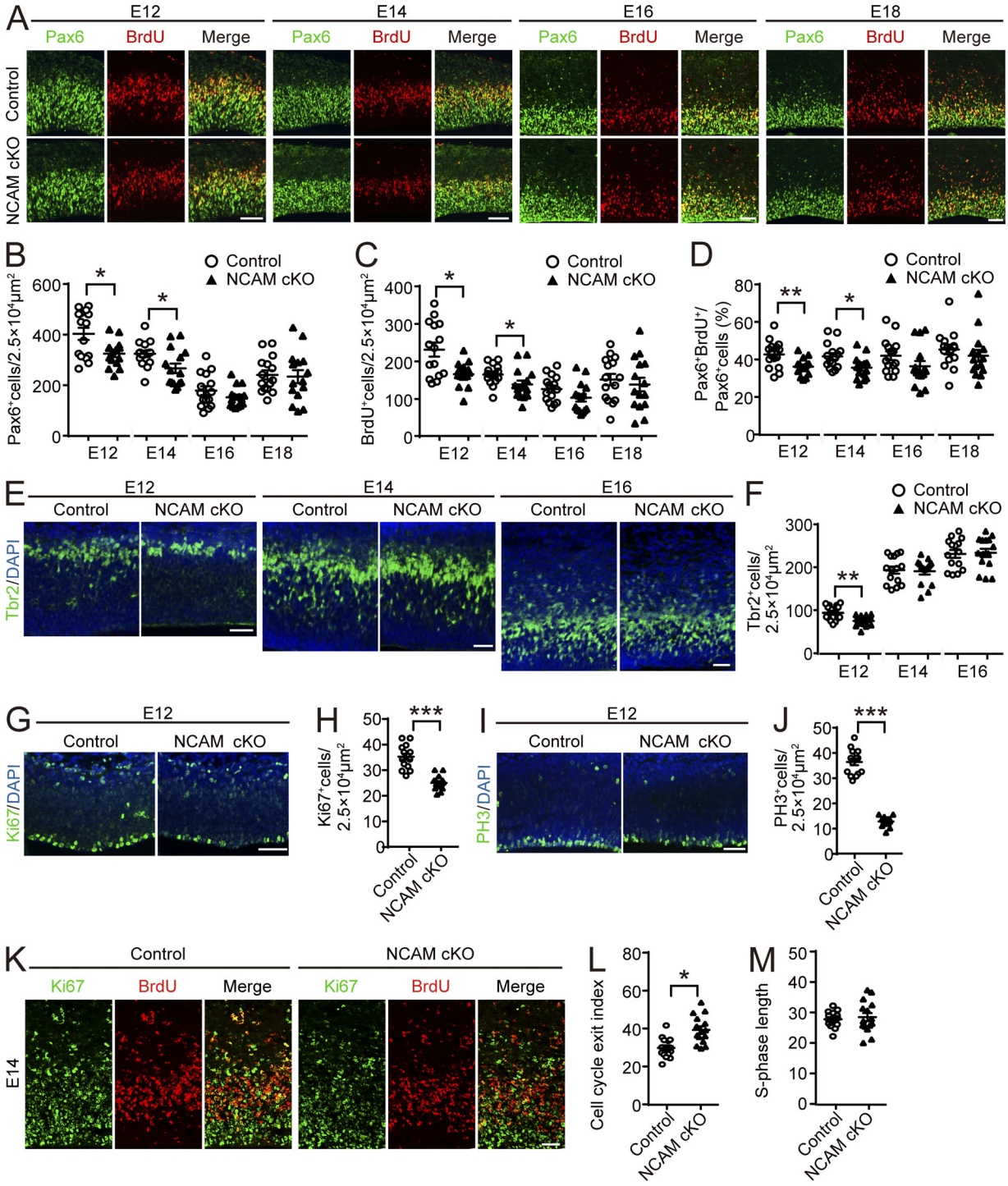

Figure 2. **NCAM deficiency transiently suppresses NPC proliferation in vivo. (A)** Coronal sections of control and NCAM-cKO cortices were coimmunostained for BrdU and Pax6 30 min after BrdU injection. **(B–D)** Numbers of Pax6⁺ (B) and BrdU⁺ (C) cells and percentages of Pax6⁺BrdU⁺ cells in total Pax6⁺ cell population (D). **(E–J)** Coronal sections of control and NCAM-cKO cortices were immunostained for Tbr2 (E), Ki67 (G), or PH3 (I) with DAPI counterstaining. Numbers of Tbr2⁺ (F), Ki67⁺ (H), and PH3⁺ (J) cells in the VZ/SVZ. **(K)** Coronal sections of E14 control and NCAM-cKO cortices were coimmunostained for BrdU and Ki67. **(L and M)** Percentages of BrdU⁺Ki67⁻ cells in the total BrdU⁺ cell population (L) and percentages of BrdU⁺Ki67⁺ cells in the total Ki67⁺ cell population (M). Scale bars, 50 µm. *n* = 15 brain slices from three mice. Values represent mean ± SEM. *, P < 0.05; **, P < 0.01; ***, P < 0.001 (two sided). Student's *t* test or Mann-Whitney test (E12 in B, E12 in C, and E14 in F).

to control levels at P7 (Fig. 3, C and F). Spatial distribution of these cortical neurons was unaltered in NCAM-cKO mice (Fig. S3), suggesting that the lower numbers of cortical neurons observed in NCAM-cKO mice are not caused by a migration defect.

Decreased numbers of both deep- and upper-layer cortical neurons at earlier developmental stages but normal levels at later developmental stages can also be explained by a delayed generation of cortical neurons in NCAM-deficient mice. To

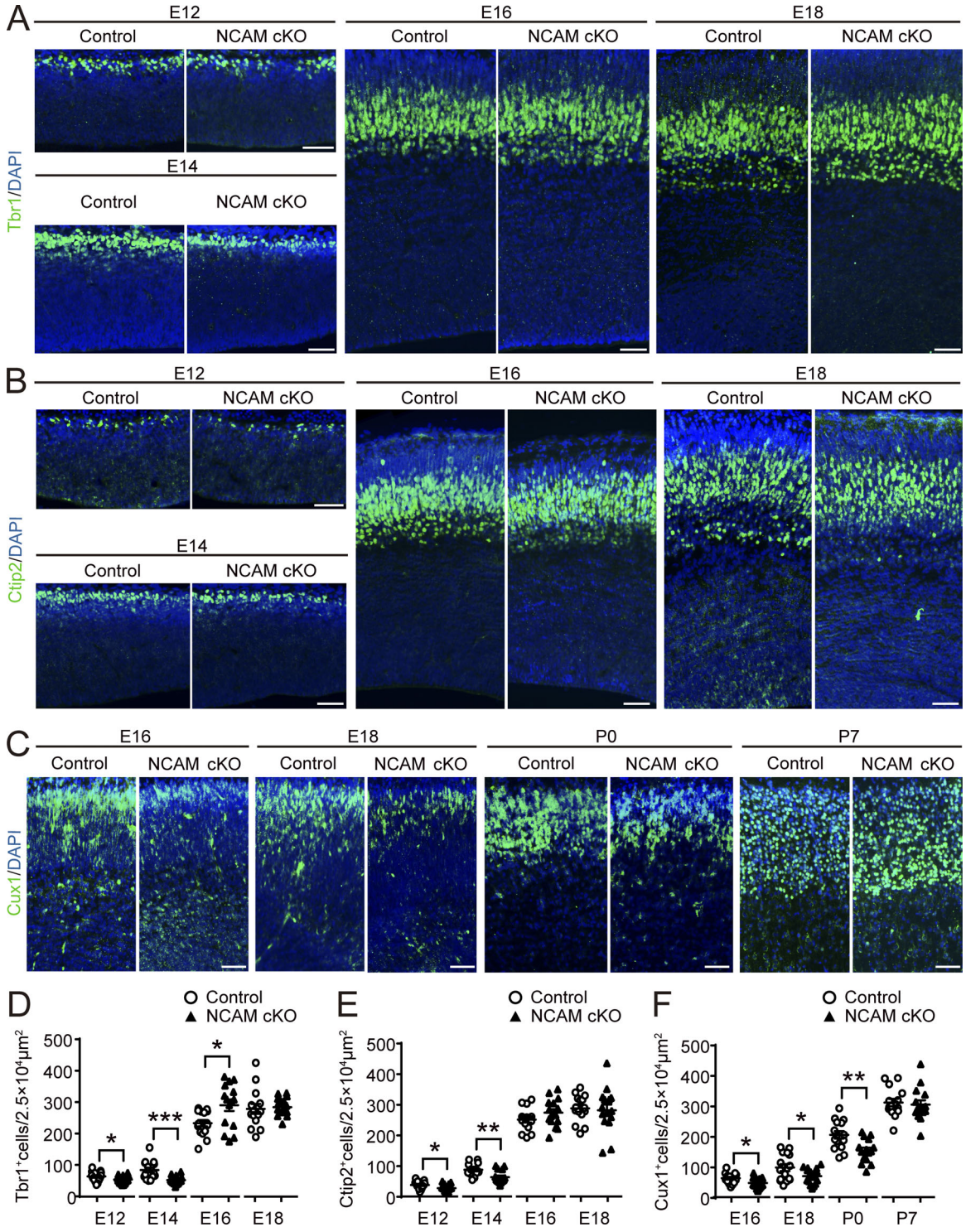

Figure 3. **NCAM deficiency reduces numbers of cortical neurons at early but not later developmental stages. (A–C)** Coronal sections of control and NCAM-cKO cortices were immunostained for Tbr1 (A), Ctip2 (B), and Cux1 (C) with DAPI counterstaining. Scale bars, 50 µm. **(D–F)** Numbers of Tbr1⁺ (D), Ctip2⁺ (E), and Cux1⁺ (F) cells per 2.5 × 10^4 µm². *n* = 15 brain slices from three mice. Values represent mean ± SEM. *, P < 0.05; **, P < 0.01; ***, P < 0.001 (two sided). Student's *t* test or Mann-Whitney test (E14 in D).

assess this possibility, we performed birth-dating analysis to examine the generation date of distinct cortical neurons. Pregnant mice were injected with BrdU at E11.5, E14.5, E15.5, or E16.5. The embryos were collected at either E18 (for analysis of Tbr1⁺ and Ctip2⁺ neuron generation) or P2 (for analysis of Cux1⁺ neuron generation). The proportion of cell-specific neurons born at the time of injection (BrdU⁺marker⁺ cells/total number of marker⁺ cells) was analyzed. Generation of Tbr1⁺ and Ctip2⁺

neurons was lower at E11.5 (Fig. 4, A, B, and D), but higher at E14.5 (Fig. 4, A, B, and E), in NCAM-cKO mice. This intergenotype difference diminished at E15.5 (Fig. 4, A, B, and F), when deep-layer neuron generation is close to completion. These data aligned well with our findings that the numbers of deep-layer neurons were reduced in NCAM-cKO mice at E12 and E14, but were normal by E18 (Fig. 3, D and E). The generation of upper-layer neurons ($Cux1^+BrdU^+/Cux1^+$ cells) was reduced at E16.5 in NCAM-cKO mice (Fig. 4, C and G), which could explain the decreased numbers of upper-layer neurons from E16 to P0 (Fig. 3 F). The number of upper-layer neurons in NCAM-cKO mice was normal at P7 (Fig. 3 F), indicating a postnatal "rescue" generation of upper-layer neurons. In summary, these data strongly indicate that NCAM regulates the temporal generation of cortical neurons.

NCAM deficiency leads to precocious gliogenesis

We further examined whether NCAM regulates the temporal generation of glial cells. More glial fibrillary acidic protein–positive ($GFAP^+$) cells were observed in NCAM-cKO mice than in control littermates at E18 and P0 (Fig. 5, A and B). Interestingly, $GFAP^+$ cells were observed in the VZ/SVZ of NCAM-cKO mice at E16 (Fig. 5, A and C), whereas fewer $GFAP^+$ cells were observed in control brains at this stage because astrocytes normally do not appear before E18 (Miller and Gauthier, 2007; Molofsky et al., 2012). These results indicate an earlier appearance of astrocytes in NCAM-cKO mice. The intergenotype difference diminished at P7, when astrocyte generation is close to completion (Wang and Bordey, 2008; Fig. 5, A and B). Birth-dating analysis of astrocytes by BrdU pulse labeling at the onset of their generation at E16.5 (Miller and Gauthier, 2007) and calculating the numbers of $BrdU^+GFAP^+$ cells at P2 revealed more $BrdU^+GFAP^+$ cells in NCAM-cKO mice (Fig. 5, D and E), indicating an increased generation of astrocytes at E16.5 in NCAM-cKO mice. Numbers of $Olig2^+$ oligodendrocytes were increased in NCAM-cKO brains at E18, but similar to those in control mice at P0 (Fig. 5, F and G). Birth-dating analysis of oligodendrocytes by BrdU pulse labeling at E16.5 showed that the percentage of $BrdU^+Olig2^+$ cells was increased in NCAM-cKO mice at P2 (Fig. 5, H and I). Consistent with these results, numbers of cells expressing brain lipid–binding protein (BLBP; Fig. 5, L and M), which is initially expressed in RGCs and later becomes restricted to astrocytes (Feng et al., 1994; Kurtz et al., 1994), as well as numbers of cells expressing A2B5, a marker of immature glial restricted progenitors (Baracskay et al., 2007; Dietrich et al., 2002; Fig. 5, J and K), were increased in the brains of NCAM-cKO mice at E14 and E16, respectively. This increase was not due to an expansion of the RGC pool, because the numbers of $Pax6^+$ RGCs were reduced at E14 and reached normal levels at E16 (Fig. 2, A and B). Thus, the increase in numbers of $BLBP^+$ and $A2B5^+$ cells is likely due to an enhanced glial progenitor density, reflecting an earlier glial specification. Taken together, these results suggest that NCAM deficiency in NPCs results in precocious gliogenesis.

Profilin2 binds to NCAM

To investigate the molecular mechanisms underlying NCAM-dependent cortical development, yeast two-hybrid screening was performed with NCAM140 as a bait (Li et al., 2013). NCAM140 in NPCs is expressed at higher levels relative to other isoforms (Prodromidou et al., 2014). Among >2 × 10^6 clones screened, 26 clones were positive. A BLAST database search (http://www.ncbi.nlm.nih.gov/BLAST/) indicated that one clone, encoding full-length profilin2, was in the correct open reading frame. To confirm the association between NCAM and profilin2, NCAM was immunoprecipitated from neonatal brain homogenates using polyclonal antibodies recognizing NCAM extracellular domain. Western blot analysis showed that profilin2 was coimmunoprecipitated by NCAM antibodies. Inversely, NCAM120, NCAM140, NCAM180, and soluble NCAM105 were coimmunoprecipitated by profilin2 antibodies (Fig. 6 A). Direct binding was assessed by ELISA, with profilin2 being substrate-coated and probed by the recombinantly expressed intracellular domains of NCAM140 and NCAM180. NCAM140, but notably not NCAM180, bound to profilin2 in a concentration-dependent and saturable manner (Fig. 6 B). Identification of profilin2-binding sites in NCAM revealed that peptides encoding aa729–750 and aa748–763 bound to profilin2 (Fig. 6 C). These two peptides had three overlapping amino acids: asparagine (N^{748}), leucine (L^{749}), and cysteine (C^{750}). To investigate whether these amino acids mediated the binding to profilin2, binding of profilin2 to a nonmutated $^{745}IAVNLCGKA^{753}$ peptide comprising the NLC motif and two mutated peptides (with two of these three amino acids changed at a time) was analyzed. Mutation of L^{749} and C^{750} into alanine (A^{749}) and serine (S^{750}) completely blocked the binding to profilin2 (Fig. 6 D). Mutation of N^{748} and L^{749} into glutamine (Q^{748}) and A^{749} partially suppressed the interaction, suggesting that N^{748} is not crucial for it (Fig. 6 D). Mutation of $^{749}LC^{750}$ in the recombinant intracellular domain of NCAM140 to $^{749}AS^{750}$ also abolished its binding to profilin2 as tested by ELISA, confirming that L^{749} and C^{750} are essential for the binding of NCAM140 to profilin2 (Fig. 6, E and F).

Profilin2 exhibits an expression pattern similar to that of NCAM in the developing cortex

To analyze whether NCAM colocalizes with profilin2 in the developing cortex, cortical sections of E12–P0 wild-type mice were coimmunostained for NCAM, profilin2, and Sox2 (Fig. 6 G) or Tuj1 (Fig. 6 H). Profilin2 colocalized with NCAM at all developmental stages analyzed, exhibiting an expression pattern similar to that of NCAM (Fig. 6, I and J; and Fig. S5 B). Although profilin2 levels increased in the whole brain during development (Fig. S1, A and G), both the average profilin2 immunofluorescence density in VZ/SVZ (Fig. 6 I) and the percentage of profilin2 immunofluorescence intensity in VZ/SVZ relative to that in the total dorsal brain (Fig. 6 J) decreased. This was particularly evident in the gliogenic period. Profilin2 protein (Fig. 6, K and L) and mRNA (Fig. 6 M) expression were reduced in NCAM-cKO versus wild-type NPCs, suggesting that NCAM regulates profilin2 expression and further implying the functional relationship between these two proteins.

Profilin2 is required for NCAM-dependent NPC proliferation and differentiation

To explore whether NCAM controls the proliferation of NPCs through profilin2, BrdU incorporation was analyzed in cultured

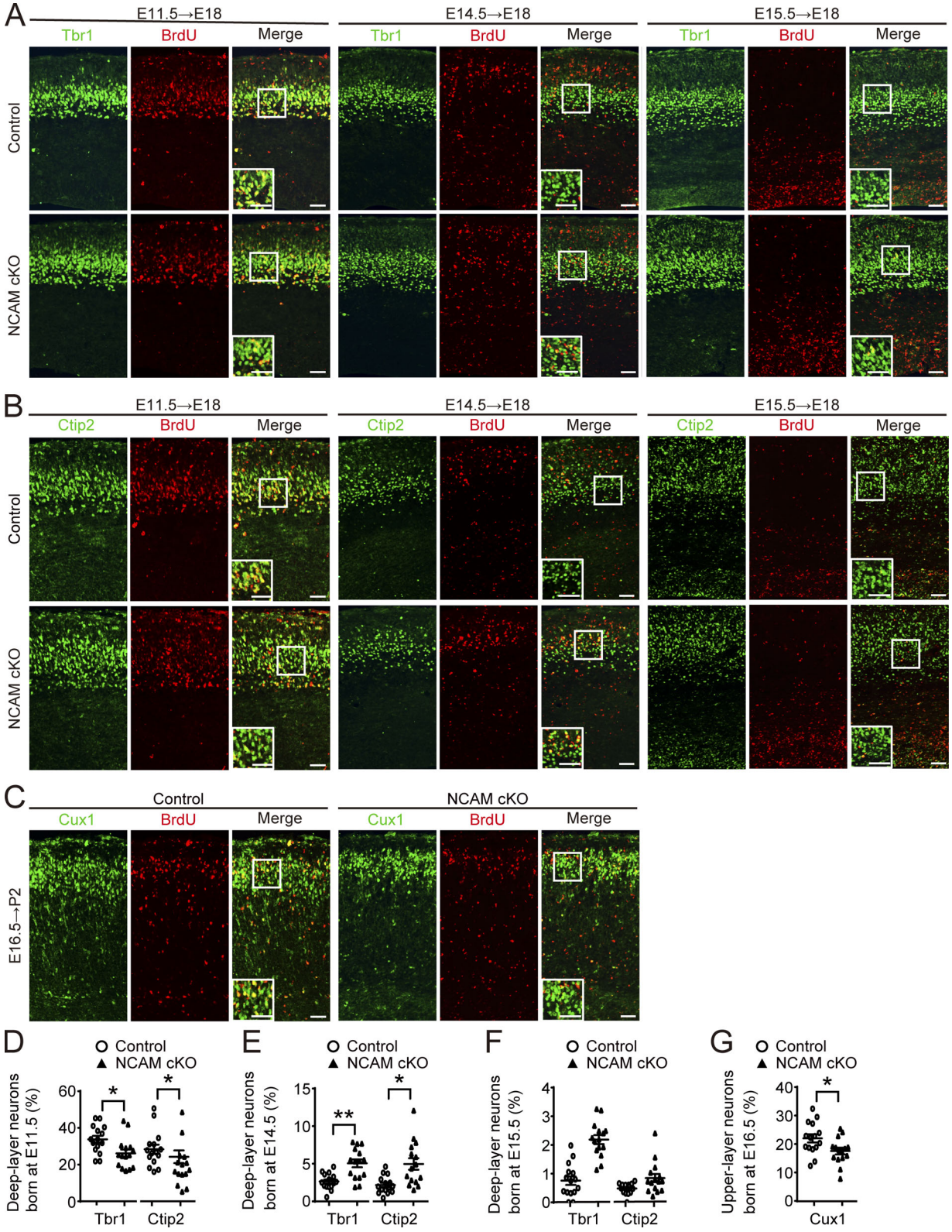

Figure 4. **NCAM deficiency delays the generation of cortical neurons in vivo. (A and B)** Cortical sections of E18 control and NCAM-cKO mice were coimmunostained for BrdU and Tbr1 (A) or Ctip2 (B). BrdU was injected at E11.5, E14.5, or E15.5. **(C)** Cortical sections of P2 control and NCAM-cKO mice were coimmunostained for BrdU and Cux1. BrdU was injected at E16.5. Scale bars, 50 µm. **(D–G)** Percentages of BrdU$^+$Tbr1$^+$, BrdU$^+$Ctip2$^+$, or BrdU$^+$Cux1$^+$ cells in total populations of Tbr1$^+$, Ctip2$^+$, or Cux1$^+$ cells after BrdU administration at E11.5 (D), E14.5 (E), E14.5 (F), or E16.5 (G). *n* = 15 brain slices from three mice. Values represent mean ± SEM. *, P < 0.05; **, P < 0.01 (two sided). Student's *t* test or Mann-Whitney test (BrdU$^+$Ctip2$^+$ cells in E and F).

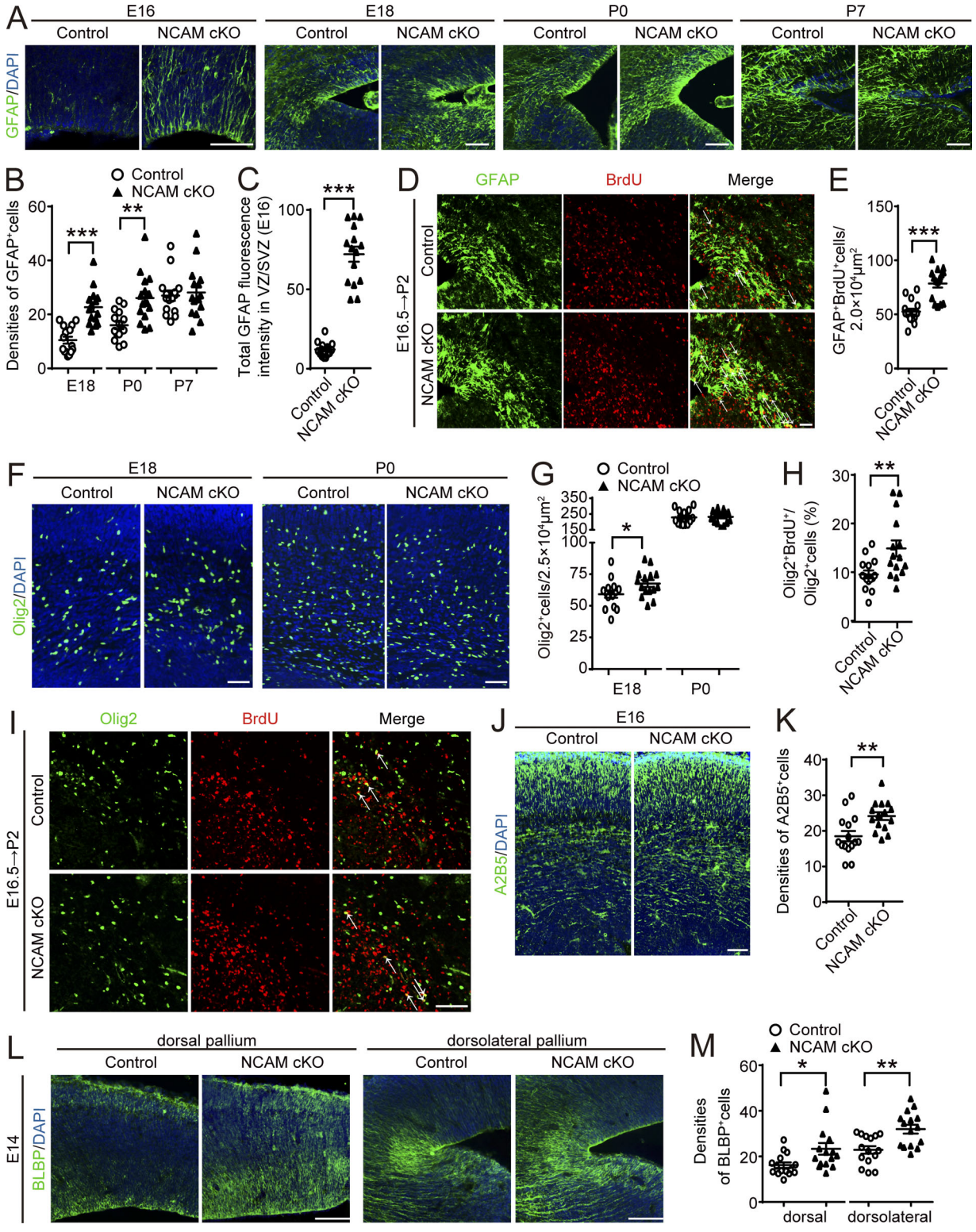

Figure 5. **NCAM deficiency results in precocious gliogenesis. (A)** Coronal sections of the VZ were immunostained for GFAP with DAPI counterstaining. **(B)** Densities of GFAP⁺ cells in the dorsolateral VZ. **(C)** Total intensity of GFAP labeling per E16 VZ/SVZ. **(D)** Coronal sections of the dorsolateral VZ of P2 control and NCAM-cKO mice were coimmunostained for BrdU and GFAP. BrdU was injected at E16.5. **(E)** Numbers of BrdU⁺GFAP⁺ cells per 2.0 × 10^4 μm² in the dorsolateral VZ. **(F)** Coronal cortical sections of E18 and P0 control and NCAM-cKO mice were immunostained for Olig2 with DAPI counterstaining. **(G)** Numbers of Olig2⁺ cells per 2.5 × 10^4 μm². **(H)** Percentages of BrdU⁺Olig2⁺ cells in the total Olig2⁺ cell population. **(I)** Coronal sections of the dorsal VZ of P2 control and NCAM-cKO mice were coimmunostained for BrdU and Olig2. BrdU was injected at E16.5. **(J)** Cortical sections of E16 control and NCAM-cKO mice were immunostained for A2B5 with DAPI counterstaining. **(K)** Densities of A2B5⁺ cells. **(L)** Cortical sections of E14 control and NCAM-cKO mice were immunostained for BLBP⁺ with DAPI counterstaining. **(M)** Densities of BLBP⁺ cells. Scale bars, 50 μm. *n* = 15 brain slices from three mice. Values represent mean ± SEM. *, P < 0.05; **, P < 0.01; ***, P < 0.001 (two sided). Student's *t* test or Mann-Whitney test (C and H).

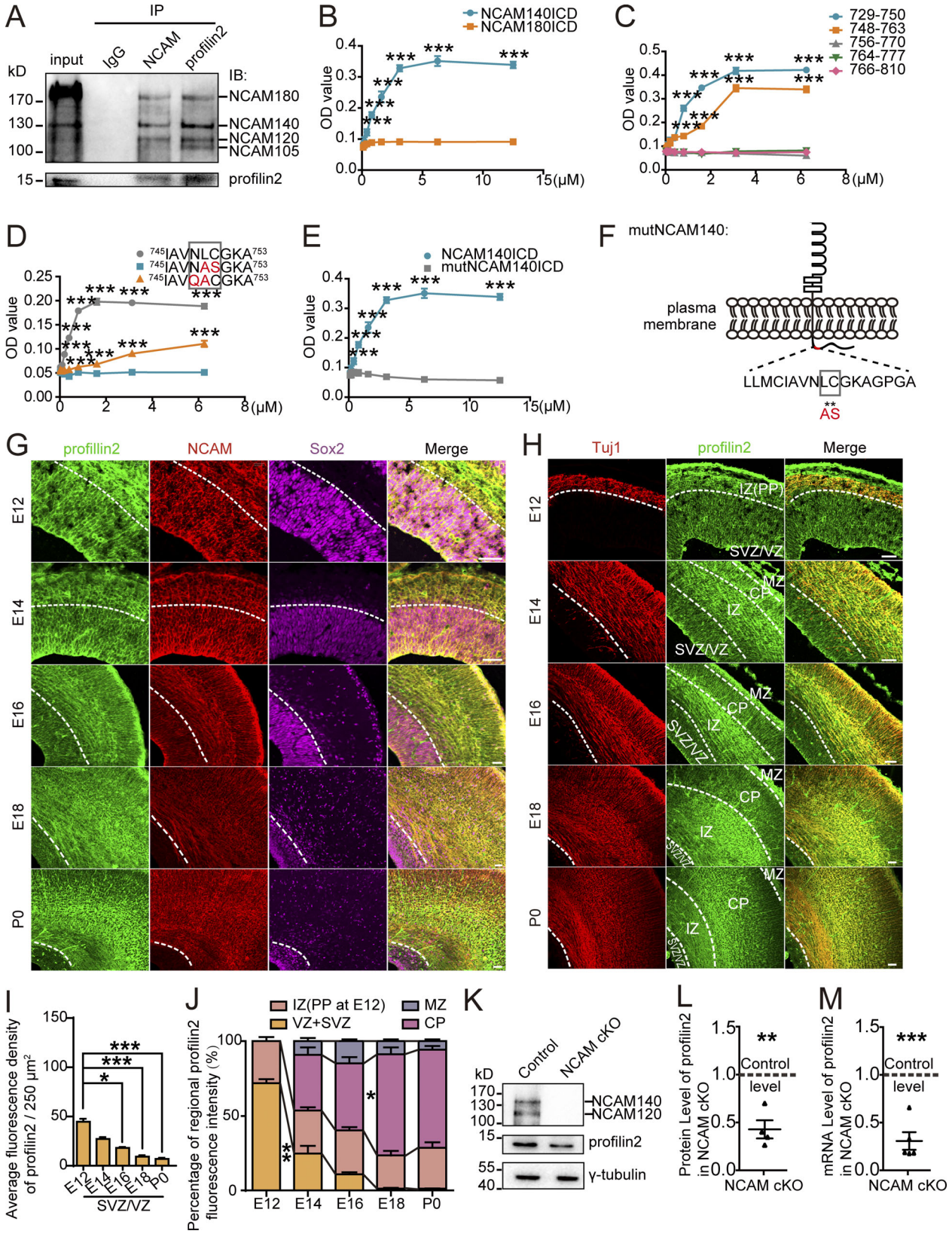

Figure 6. **Profilin2 is a novel binding partner of NCAM. (A)** Coimmunoprecipitation analysis of the interaction between NCAM and profilin2 using P0 mouse brain homogenates. **(B)** ELISA analysis of the binding of NCAM140ICD or NCAM180ICD to immobilized profilin2. **(C–E)** ELISA of the binding of biotinylated NCAM140ICD-derived peptides (C), wild-type NCAM140 (aa745–753) peptide and its mutant variants with ^{749}LC^{750} mutated to ^{749}AS^{750} or ^{748}NL^{749} mutated to ^{748}QA^{749} (D), and wild-type NCAM140ICD or mutNCAM140ICD (^{749}LC^{750} to ^{749}AS^{750} mutation; E) to immobilized profilin2. *n* = 3 biological replicates. **(F)** Schematic diagram of amino acid mutations in mutNCAM140ICD. **(G and H)** Coronal sections of the VZ (G) and the cortex (H) of control mice were

coimmunostained for profilin2, NCAM, and Sox2 (G) or Tuj1 (H). Scale bars, 50 µm. **(I)** Average profilin2 immunofluorescence density in each layer. **(J)** Percentages of profilin2 immunoreactivity in each layer. *n* = 9 brain slices from three mice. **(K and L)** Western blot analysis of levels of NCAM and profilin2 in cultured NPCs derived from E14 control and NCAM-cKO VZ/SVZ (K). The relative levels of profilin2 protein in NCAM-cKO NPCs, with the profilin2 levels in control NPCs set to 100% (L). *n* = 4 biological replicates. **(M)** Quantitative PCR analysis of the levels of profilin2 mRNA in cultured NPCs derived from E14 control and NCAM-cKO brains. Profilin2 mRNA levels in control NPCs were set to 100%. *n* = 5 biological replicates. Values represent mean ± SEM. *, P < 0.05; **, P < 0.01; ***, P < 0.001 (two sided). Two-way ANOVA (B–E), one-way ANOVA with Bonferroni correction (IZ, CP, and MZ in J), Dunnett's T3 correction (VZ/SVZ in J), Kruskal-Wallis test with Dunn-Bonferroni correction (I), and paired *t* test (L and M).

NPCs transfected with either profilin2 siRNA (siProfilin2) or control (scrambled) siRNA (NC). NPCs were analyzed after incubation with or without NCAM antibodies recognizing NCAM extracellular domain and triggering downstream signaling of NCAM (Li et al., 2013). Transfection of siProfilin2 suppressed profilin2 (Fig. S4, A–C) but not profilin1 expression (Fig. S4D) in Neuro-2a cells and NPCs, and it decreased NPC proliferation (Fig. 7, A and C; siProfilin2-399). Incubation with NCAM antibodies increased proliferation of NPCs transfected with control siRNA, but not of NPCs transfected with siProfilin2 (Fig. 7, A and C). This indicates that NCAM promotes the proliferation of NPCs through profilin2.

To investigate whether profilin2 plays a role in NCAM-dependent differentiation of NPCs, NC- or siProfilin2 (siProfilin2-399)-transfected NPCs were allowed to differentiate in the absence or presence of NCAM antibodies for 5 d. Immunofluorescence analysis showed that the percentages of Tuj1$^+$ cells (Fig. 7, B and D) were decreased, whereas the percentages of GFAP$^+$ (Fig. 7, E and G) and O4$^+$ cells (Fig. 7, F and H) were increased by profilin2 knockdown. These observations indicate that profilin2, similar to NCAM, promotes neuronal differentiation and suppresses differentiation of NPCs into glial cells. Consistent with in vivo results, NCAM antibody treatment increased the percentages of Tuj1$^+$ cells (Fig. 7, B and D) but decreased GFAP$^+$ (Fig. 7, E and G) and O4$^+$ cell percentages (Fig. 7, F and H) in NC-transfected NPCs. However, the effect of NCAM antibodies on neuronal and astroglial differentiation was abolished in NPCs transfected with siProfilin2 (Fig. 7, B, D, E, and G), indicating that profilin2 is required for NCAM-dependent regulation of neuronal and astroglial differentiation. Profilin2 knockdown reduced but did not abolish the suppressing effect of NCAM antibodies on oligodendroglial differentiation (Fig. 7, F and H). To further confirm that profilin2 is involved in NCAM-regulated NPC differentiation in a cell-autonomous manner, NPCs were transfected with shRNA Profilin2 (shProfilin2) alone or together with shRNA-resistant profilin2 plasmids encoding GFP under a separate promotor. NPCs were then treated with NCAM antibodies. NCAM antibody–enhanced neurogenesis and NCAM antibody–decreased astrogenesis were prevented by profilin2 knockdown, which was rescued by cotransfection with shRNA-resistant profilin2 (Fig. 7, I–K). Therefore, these results indicate that profilin2 is the downstream effector of NCAM, through which NCAM regulates NPC proliferation and differentiation.

NCAM regulates actin cytoskeleton dynamics through profilin2

We further tested whether NCAM regulates NPC proliferation and differentiation through profilin2-mediated actin polymerization. Western blot analysis of total cell lysates showed that the expression of actin did not differ between control and NCAM-cKO NPCs. However, the depolymerized actin (G-actin) levels were higher in NCAM-cKO NPCs. Proportionally, the polymerized actin (F-actin) levels were reduced in NCAM-cKO NPCs (Fig. 8, A and B), indicating that NCAM promotes actin polymerization. Western blot analysis revealed that NCAM knockdown–induced reduction of the F-actin/G-actin ratio was rescued by wild-type NCAM140, but not mutNCAM (unable to bind profilin2), in mouse embryonic fibroblasts (MEFs; Fig. 8 C). To confirm these data, control and NCAM-cKO NPCs expressing GFP only, coexpressing wild-type NCAM140, or mutNCAM were stained by fluorescent phalloidin and DNase I to visualize F- and G-actin, respectively. Fluorescence microscopic analysis showed that the F-actin/G-actin ratio was reduced in NCAM-cKO NPCs. Lentiviral transduction with wild-type NCAM140, but not mutNCAM, increased the F-actin/G-actin ratio in NCAM-cKO NPCs to control levels (Fig. 8, D and E). The decreased F-actin/G-actin ratio in NCAM-cKO NPCs was also rescued by profilin2 overexpression (Fig. 8, F and G). These results indicate that NCAM promotes actin polymerization through its binding to profilin2.

The actin cytoskeleton is crucial for soma rounding, as well as for increased rigidity during cell division (Kunda and Baum, 2009). The role of NCAM in cell shape alteration was investigated in dividing cells, and the cell shape index (CSI) of NPCs was calculated in meta- and anaphase at the VZ surface. NCAM deficiency leads to elongated morphology of NPCs and reduced CSI values (Fig. 8, H and I), indicating that mitotic NPCs in NCAM-cKO mice fail to round up, which is believed to lead to the perturbation of cell cycle progression (Heng and Koh, 2010).

Immunofluorescence analysis showed reduced NPC proliferation and neurogenesis and increased astrogenesis in NCAM-cKO NPCs (Fig. 8, J–N). Transduction of NCAM-cKO NPCs with wild-type NCAM140, but not mutNCAM-expressing lentiviruses, normalized proliferation, neurogenesis, and astrogenesis (Fig. 8, J–N). Hence, NCAM controls the proliferation and differentiation of NPCs through binding to profilin2 via regulation of actin cytoskeleton dynamics.

Discussion

We demonstrated that NCAM is dynamically expressed in the developing cortex with high expression in NPCs during the neurogenic period and lower expression in NPCs in the gliogenic period. Expression of NCAM is required for maintenance of the precise proliferation and the timely generation of cortical neurons and glial cells. Furthermore, profilin2 was identified to be the mediator of NCAM-dependent regulation of cytoskeleton

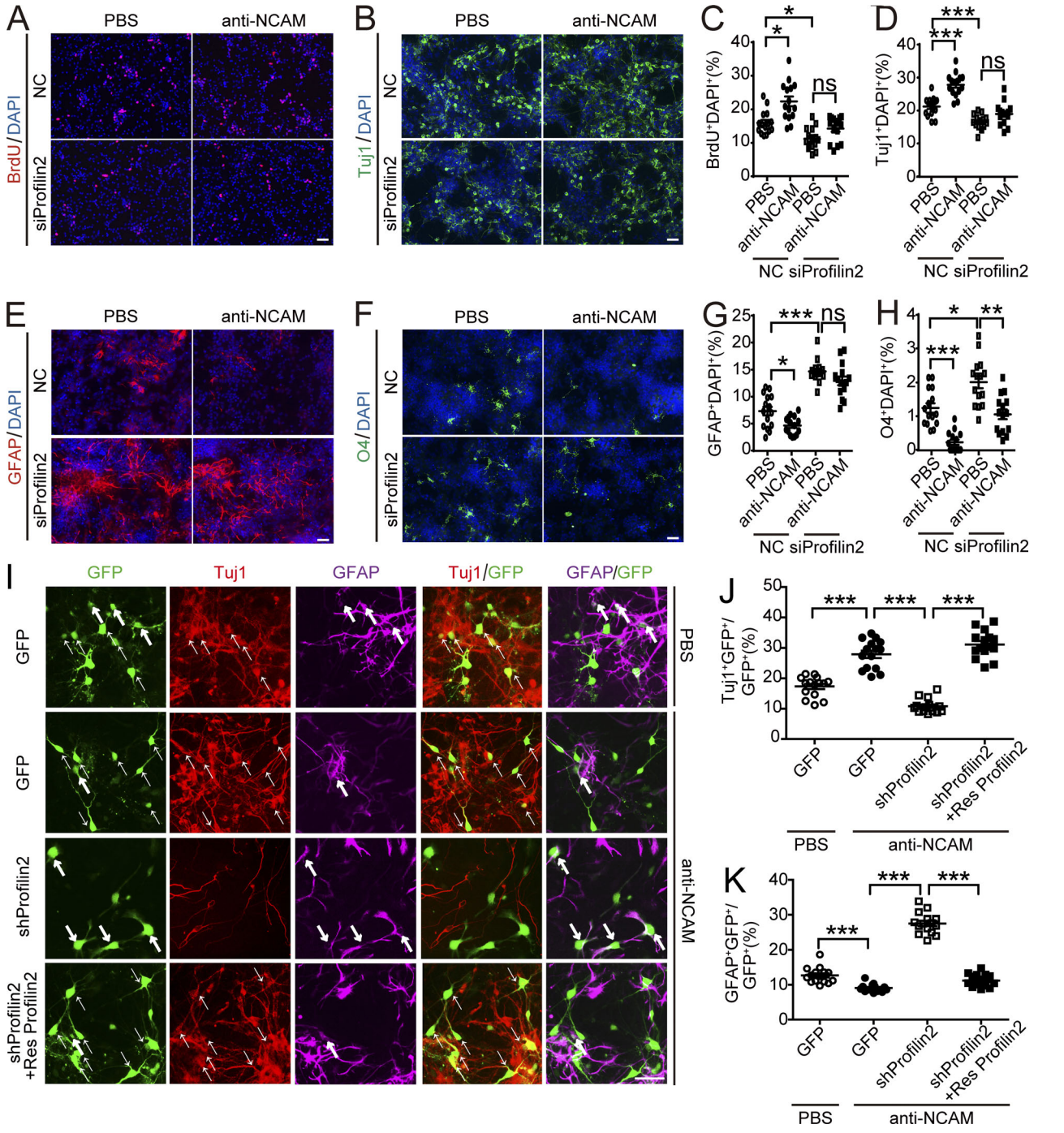

Figure 7. **NCAM enhances NPC proliferation and differentiation through profilin2. (A)** Cultured NPCs transfected with siProfilin2 or NC were incubated with NCAM antibodies and BrdU. Cells were immunostained for BrdU with DAPI counterstaining. **(B, E, and F)** Cultured NPCs transfected with siProfilin2 or NC were incubated with NCAM antibodies or PBS and cultured in differentiation condition for 5 d. Cells were immunostained for Tuj1 (B), GFAP (E), or O4 (F) and counterstained with DAPI. **(C, D, G, and H)** Percentages of $BrdU^+DAPI^+$ (C), $Tuj1^+DAPI^+$ (D), $GFAP^+DAPI^+$ (G), and $O4^+DAPI^+$ (H) cells in the total population of $DAPI^+$ cells. **(I–K)** Cultured NPCs cotransfected with profilin2 shRNA (shProfilin2) and shProfilin2-resistant plasmids (Res Profilin2), shProfilin2, or control vector expressing GFP alone (GFP) were incubated with NCAM antibodies or PBS and allowed to differentiate for 3 d. Cells were immunostained for Tuj1 or GFAP. Percentages of $Tuj1^+GFP^+$ (J) or $GFAP^+GFP^+$ (K) cells in the total population of GFP^+ cells. *n* = 15 microscopic fields from three biological replicates. Scale bars, 50 µm (A, F, and I) or 20 µm (B and E). Values represent mean ± SEM. *, P < 0.05; **, P < 0.01; ***, P < 0.001 (two sided); ns, not statistically significant. Kruskal-Wallis test with Dunn-Bonferroni post hoc correction (C) and one-way ANOVA with Bonferroni corrections (D, G, J, and K) or Dunnett's T3 correction (H).

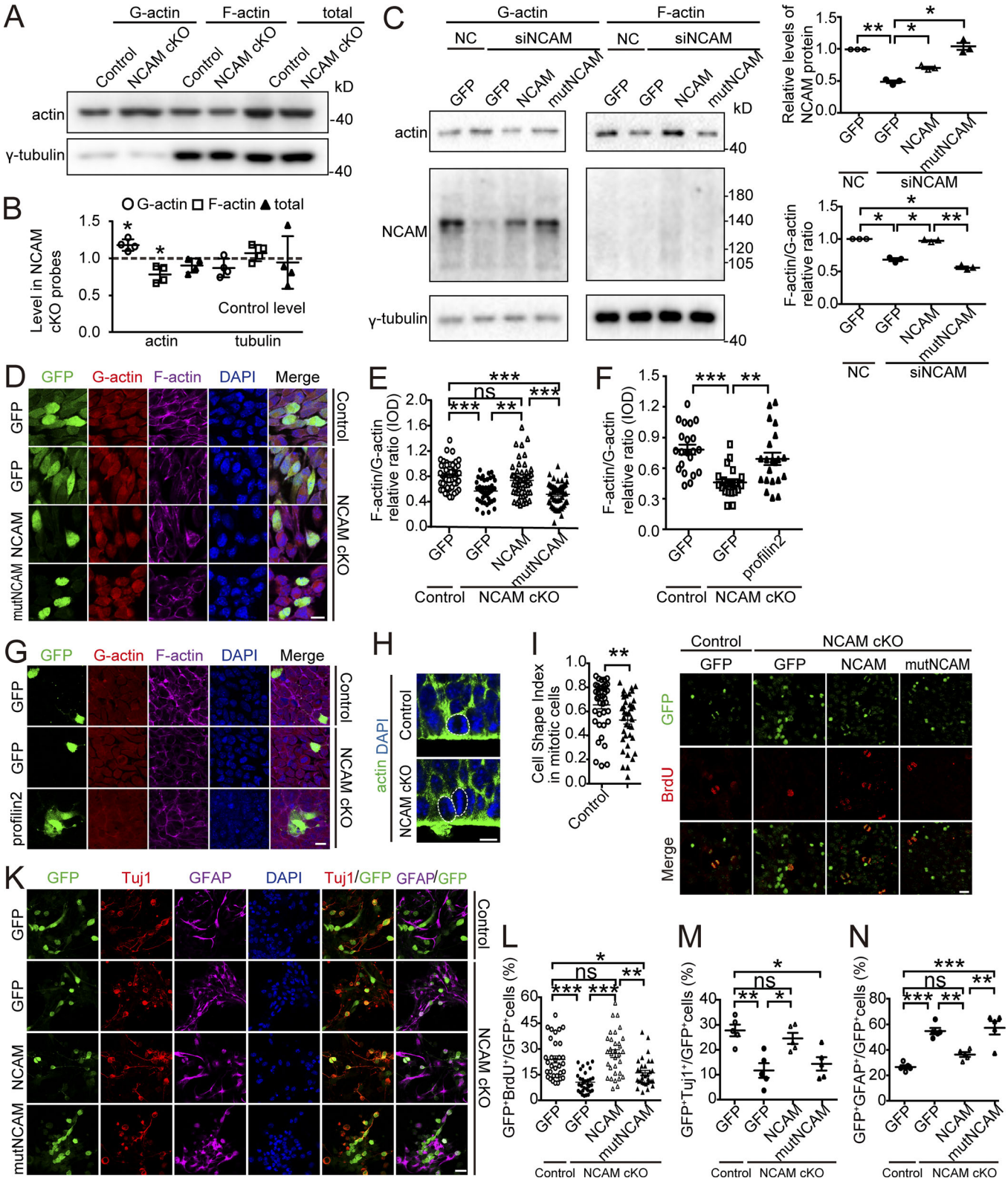

Figure 8. **NCAM enhances NPC proliferation and differentiation through profilin2-regulated actin dynamics. (A)** Western blot analysis of F- and G-actin levels in cultured control and NCAM-cKO NPCs. γ-Tubulin served as a control and was enriched in the F-actin fraction containing polymerized tubulin. **(B)** Relative levels of G- and F-actin in NCAM-cKO NPCs. The levels of G- and F-actin in control NPCs were set to 100%. *n* = 4 biological replicates. **(C)** Cultured MEFs were cotransfected with NCAM siRNA (siNCAM) or NC and with lentiviruses coexpressing GFP and wild-type NCAM140 (NCAM) or mutant NCAM140 (mutNCAM). MEFs cotransfected with NC and lentiviruses expressing GFP only served as a control. Western blot analysis of levels of NCAM, actin, and tubulin. Lysis with the F-actin stabilization buffer solubilizes and releases NCAM to the G-actin fraction. Relative levels of NCAM protein in the G-actin fraction and the relative ratio of G- and F-actin were quantified. *n* = 3 biological replicates. **(D)** Cultured NCAM-cKO NPCs were transduced with lentiviruses coexpressing GFP

and NCAM or mutNCAM. NPCs transduced with lentiviruses expressing GFP only served as a control. NPCs were stained by fluorescent phalloidin to visualize F-actin and by DNase I to visualize G-actin. **(E and F)** F-actin/G-actin ratios in cells are shown in D and G, respectively. *n* = 54 cells (E) and 21 cells (F) from three biological replicates. **(G)** Cultured NCAM-cKO NPCs were transduced with plasmids coencoding either GFP or profilin2 and GFP, and then they were stained with fluorescent phalloidin and DNase I. **(H)** Coronal VZ sections of E12 control and NCAM-cKO mice were immunostained for actin with DAPI counterstaining. White dotted lines show examples of cell boundaries. **(I)** The CSI for dividing cells in the VZ. *n* = 40 mitotic cells from three mice. **(J and K)** Cultured NCAM-cKO NPCs were transduced with lentiviruses coexpressing GFP and NCAM or mutNCAM, incubated with BrdU, and immunostained for BrdU with DAPI counterstaining (J). Cultured NPCs differentiated for 5–7 d were immunostained for Tuj1 and GFAP with DAPI counterstaining (K). **(L–N)** Percentages of $BrdU^+GFP^+$ (L), $Tuj1^+GFP^+$ (M), and $GFAP^+GFP^+$ (N) cells in total GFP^+ cell population. *n* = 32 microscopic fields from three biological replicates (L). *n* = 5 biological replicates (M and N). Scale bars, 20 µm (D, G, J, and K) or 5 µm (H). Values represent mean ± SEM. *, P < 0.05; **, P < 0.01; ***, P < 0.001 (two sided); ns, not statistically significant. Paired *t* test (B), Mann-Whitney test (I), one-way ANOVA with Dunnett's T3 correction (C) or Bonferroni correction (M and N), and Kruskal-Wallis test with Dunn-Bonferroni post hoc comparisons (E, F, and L).

dynamics controlling NPC proliferation and differentiation during cortical development (Fig. 9).

Previous studies suggested that NCAM can function as both a cell-extrinsic and cell-intrinsic signaling molecule in NPCs (Amoureux et al., 2000; Boutin et al., 2009; Kim and Son, 2006; Klein et al., 2014; Prodromidou et al., 2014). The present study confirms these views by showing that specific ablation of NCAM expression in NPCs suppressed proliferation and enhanced cell cycle exit of NPCs at the earlier neurogenic stage, leading to a transiently reduced NPC pool. At later developmental stages (i.e., from E16 onward), neither proliferation of NPCs nor NPC numbers in NCAM-mutant mice were different from those in wild-type mice. Interestingly, NCAM expression in NPCs was reduced from E16 onward, showing considerably reduced levels at the gliogenic period. Thus, the loss of NCAM-dependent regulation of NPC proliferation at later developmental stages may be due to the decline in NCAM expression. However, the fact that the transiently decreased proliferation in the earlier neurogenic period does not lead to an ultimately depleted NPC pool at later developmental stages also suggests a compensatory mechanism.

During brain development, a number of cell cycle regulators are involved in cell fate specification, whereas key factors for cell fate specification influence cell cycle (Politis et al., 2008). In

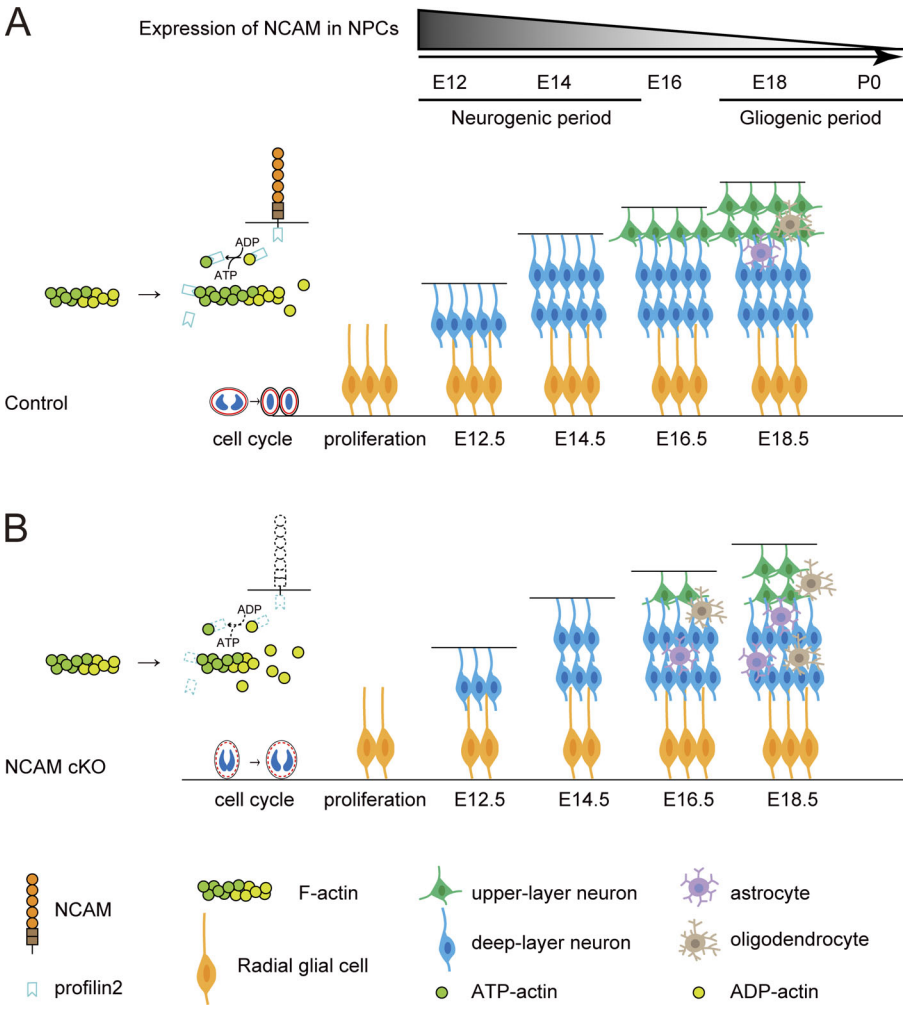

Figure 9. **The role of NCAM in regulating the temporal generation of neurons and glia in the developing cortex. (A)** NCAM expression is high in NPCs at the neurogenic period and declines at the gliogenic period. The intracellular domain of NCAM interacts with profilin2 and promotes actin polymerization in NPCs. NCAM-dependent actin regulation is required for rounding of NPCs during mitosis as well as control of NPC proliferation and temporal differentiation into cortical neurons and glia. **(B)** Ablation of NCAM expression in NPCs results in reduced expression of profilin2 and loss of its NCAM-dependent regulation, leading to decreased actin polymerization and reduced rounding of mitotic NPCs. This slows down cell cycle progression, reduces NPC proliferation at an early stage of neural development, delays production of cortical neurons, and leads to precocious formation of cortical glia.

line with this notion, we observed a delayed generation of both upper- and deep-layer cortical neurons and a precocious gliogenesis in NCAM-mutant mice. Furthermore, the transiently increased cell cycle exit upon NCAM deletion is paralleled by increased numbers of glial progenitors during the neurogenic period, suggesting that cells exiting the cell cycle at E14 may adopt a glial fate. Consistently, GFAP$^+$ astrocytes were observed in NCAM-cKO brains as early as E16, despite the fact that astrocytes normally do not appear in rodent brains until E18 (Miller and Gauthier, 2007). Hence, it is likely that precocious astrogenesis is due to depletion of NCAM in NPCs at early rather than later developmental stages when NCAM expression in NPCs decreases. Gliogenesis is suppressed during the neurogenic period and induced after neurons have been generated in sufficient numbers (Sloan and Barres, 2014). However, NCAM-cKO mice exhibit a delayed neurogenesis. Thus, it is unlikely that the precocious astrogliogenesis observed in NCAM-cKO mice is due to the delayed generation of neurons. Moreover, transfection of plasmids encoding NCAM decreased astrogliogenesis from cultured NCAM-cKO NPCs, further confirming a cell-autonomous mechanism. Thus, we propose that NCAM, which is highly expressed in NPCs during the neurogenic period, promotes neurogenesis and suppresses gliogenesis (Fig. 9).

We provide evidence that NCAM regulates the proliferation and differentiation of NPCs via its binding to profilin2, which interacts directly with NCAM140 intracellular domain. NCAM180, NCAM120, and the soluble extracellular domain of NCAM also coimmunoprecipitate with profilin2, most likely due to their homophilic binding to NCAM140 (Soroka et al., 2003). Surprisingly, NCAM180 does not bind directly to profilin2, although NCAM140 and NCAM180 comprise overlapping aa sequences in their intracellular domains, suggesting that NCAM180 is conformationally restricted from its interaction with profilin2. NCAM180 accumulates at contacts between cells, and a reduction in its association with the actin filament–remodeling proteins may be important for stabilization of cell contacts (Pollerberg et al., 1986). In contrast, NCAM140 is more involved in dynamic cell interactions. NCAM120 and NCAM140 are the predominant forms of NCAM in NPCs at E14 (Fig. 6 K; Prodromidou et al., 2014), whereas NCAM180 and NCAM140 are the major isoforms in neurons (Korshunova et al., 2007). Consistently, NCAM140, but not its mutant with abolished binding to profilin2, rescues abnormal proliferation and differentiation of NPCs caused by NCAM depletion in NPCs. Thus, the combined observations suggest that NCAM-dependent regulation of neuronal development is fine-tuned by the temporally specific expression patterns of NCAM isoforms.

Regulation of actin dynamics by profilin1 and profilin2 require both discrete and cooperative activities. One example is that expression of profilin1 rescues the loss of spines (but not dendritic complexity) caused by profilin2 knockdown (Michaelsen et al., 2010). Indeed, profilin2-deficient neurons show an initial, transient increase in the number of sprouting neurites, which may be due to the compensatory function of profilin1 (Da Silva et al., 2003). In addition, NCAM-depleted NPCs exhibit reduced profilin2 levels. Thus, the transient nature of abnormalities in NPCs observed in NCAM-cKO cells may be due to a functional compensation by profilin1. We herein show that profilin2 is required for NCAM-regulated NPC proliferation and differentiation, which depend on binding of NCAM to profilin2, which exhibits an expression profile similar to that of NCAM in NPCs during brain development. Acute profilin2 knockdown in cultured NPCs results in a phenotype comparable to that of NCAM-deficient NPCs, suggesting that profilin2 and NCAM have similar roles in the developing cerebral cortex. Consistently, profilin2-deficient mice are hyperactive and show increased exploratory behavior (Pilo Boyl et al., 2007), thus partly resembling behavioral abnormalities in NCAM-deficient mice. Profilins bind to various ligands and are involved in distinct cellular processes, such as membrane and vesicle trafficking, endocytosis, and receptor clustering. Profilins are also found in the cell nucleus, where they may be involved in chromatin remodeling and transcription (Witke, 2004). Further research is required for a more holistic understanding of the role of profilin2 during cortical development.

NCAM is the major carrier of the linear homopolymer α2-8-*N*-acetylneuraminic acid (PSA), which plays a prominent role in regulation of migration and differentiation of progenitor cells during postnatal brain development (Angata et al., 2007), as well as in the adult brain (Burgess et al., 2008). We did not detect NCAM-PSA in E14 NPCs (Fig. 6 K), which is in accordance with previous studies showing that NCAM is not polysialylated during the early phases of neurogenesis in the developing brain (Bonfanti, 2006; Prodromidou et al., 2014; Seki and Arai, 1991). This in turn suggests that NCAM rather than PSA plays a key role at these early development stages.

Our observations also indicate that NCAM regulates corticogenesis by modulating actin dynamics. NCAM deficiency leads to reduced actin polymerization, elongated progenitor cell shape, and decreased mitosis (Fig. 9). Remodeling of the actin cytoskeleton during mitosis is necessary for formation of rounded cells with increased cortical rigidity (Heng and Koh, 2010; Luxenburg et al., 2011). At the end of mitosis, actin rearranges at cleavage furrows and contributes to formation of the contractile ring, which is crucial for cytokinesis. Another mitotic event requiring actin dynamics is centrosome separation, which depends on the flow of submembrane actin and the myosin network (Heng and Koh, 2010). The modulation of cell shape changes in coordination with cell cycle progression is a prerequisite for the acquisition of appropriate cell fates and the transformation of proliferating, undifferentiated progenitors into fully differentiated, functional cells (Cremisi et al., 2003). We show that NCAM-dependent actin remodeling promotes neurogenesis but suppresses gliogenesis.

The actin cytoskeleton is also involved in transcription control (Miralles and Visa, 2006). Actin is a component of the transcription apparatus, chromatin-remodeling complexes, and RNA-processing machinery (Miralles and Visa, 2006). Our data show that deficiency in NCAM results in inhibited neurogenesis and enhanced gliogenesis from NPCs, suggesting a role for NCAM in the control of the neurogenic–gliogenic switch. This cell fate programming comprises specific signaling pathways, such as JAK-STAT–, Notch-, BMP-, and MEK-ERK–dependent signaling to activate transcription factors (Miller and Gauthier,

2007). Whether NCAM regulates transcription by modulating actin dynamics is a question for future investigation.

In the developing brain, neurons are generated first, while gliogenesis is suppressed during the neurogenic period. Astrogliogenesis is induced later, after neurons had been generated in sufficient numbers (Sloan and Barres, 2014). Astrocytes, in turn, guide appropriate neurite and synapse development (Jacobs and Doering, 2010; Sloan and Barres, 2014). This temporal sequence of coordinated generation of neurons and astrocytes is required for proper establishment of neural circuits. Perturbations in the temporally orchestrated generation of neurons and glia may cause impaired neuronal development and synaptic plasticity, leading to neurodevelopmental disorders, such as Down syndrome, autism spectrum disorder, and "RASopathies" (Jacobs and Doering, 2010; Sloan and Barres, 2014; Zdaniuk et al., 2011), the latter including Noonan syndrome (Tartaglia et al., 2001), neurofibromatosis 1 (Hegedus et al., 2007), Costello syndrome (Paquin et al., 2009), and cardiofaciocutaneous syndrome (Urosevic et al., 2011). Despite a broad spectrum of clinical manifestations, these syndromes share some degree of mental impairment and precocious astrogenesis (Sloan and Barres, 2014). In turn, NCAM-deficient mice display hyperactivity, increased aggression, learning deficits, and impaired nest-building behaviors (Cremer et al., 1994; Stork et al., 1997, 2000, 1999; Vicente et al., 1997).

In the mature brain, NCAM is involved in regulation of the number, structure, and molecular composition of synapses, synaptic vesicle recycling, synaptic plasticity, learning (Bukalo et al., 2004; Puchkov et al., 2011; Shetty et al., 2013; Sytnyk et al., 2006), and behavior (Brandewiede et al., 2014; Kohl et al., 2013; Pillai-Nair et al., 2005; Stork et al., 1999). By regulating actin polymerization (Schlüter et al., 1997), profilin2 also plays a role in modulation of synaptic vesicle exocytosis, neuronal excitability (Pilo Boyl et al., 2007), spine density, dendritic complexity (Da Silva et al., 2003; Michaelsen et al., 2010; Witke et al., 1998), learning, and memory consolidation (Lamprecht et al., 2006). Whether NCAM and profilin2 cooperate in regulation of synapse formation and function is, however, unknown and remains a question for further investigation.

Our study suggests that abnormalities in temporal NPC fate decision can contribute to the pathophysiology of neurodevelopmental diseases associated with abnormal function of NCAM. Understanding the molecular mechanisms underlying these abnormalities may help in the design of future strategies aimed at correcting neural differentiation in the affected brain.

Materials and methods

Antibodies

The following antibodies were used for immunofluorescence analysis: goat anti-Sox2 (1:150, sc-17320, RRID: AB_2286684; Santa Cruz Biotechnology), mouse anti-BrdU (1:300, MMS-139S, RRID: AB_10719257; Covance), mouse anti–βIII-tubulin (1:500, Tuj1, T5076, RRID: AB_532291; Sigma-Aldrich), mouse anti-profilin2 (1:100, 60094-2-Ig, RRID: AB_2163215; Proteintech), rabbit anti-NCAM (1:300, ANR-041, RRID: AB_2756690; Alomone Labs), rabbit anti-NCAM (1:200, 701379, RRID: AB_2532477; Thermo Fisher Scientific), rabbit anti-Pax6 (1:300, PRB-278P, RRID: AB_291612; Covance), rabbit anti-Tbr1 (1:300, ab3190, RRID: AB_2238610; Abcam), rabbit anti-Tbr2 (1:300, ab23345, RRID: AB_778267; Abcam), rabbit anti-Olig2 (1:300, ab109186, RRID: AB_10861310; Abcam), rabbit anti-GFAP (1:500, MAB360, RRID: AB_11212597; EMD Millipore), rabbit anti-PH3 (1:300, 06-570, RRID: AB_310177; EMD Millipore), rabbit anti-Ki67 (1:100, PA5-19462, RRID: AB_10981523; Thermo Fisher Scientific), rabbit anti-Ctip2 (1:300, ab28448, RRID: AB_1140055; Abcam), rabbit anti-Cux1 (1:100, sc-13024, RRID: AB_2261231; Santa Cruz Biotechnology), rabbit anti-BLBP (1:100, ab32423, RRID: AB_880078; Abcam), mouse anti-A2B5 (1:300, MA1-90445, RRID: AB_1954783; Thermo Fisher Scientific), and rabbit anti–cleaved caspase3 (1:300, 9661, RRID: AB_2341188; Cell Signaling Technology). Rabbit anti-NCAM (ANR-041, RRID: AB_2756690; Alomone Labs) and rabbit anti-profilin2 (ab174322, RRID: AB_2783646; Abcam) antibodies were used for immunoprecipitation and Western blot analysis. Chicken anti-NCAM antibody (Li et al., 2013) was used to assay NPC proliferation and differentiation. Rat anti-NCAM (556323, RRID: AB_396361; BD Pharmingen) antibody was used for Western blot analysis and ELISA. Mouse anti-actin (A5441, RRID: AB_476744; Sigma-Aldrich) antibody was used for immunofluorescence and Western blot analysis. Mouse anti–γ-tubulin antibody (T6557, RRID: AB_477584; Sigma-Aldrich) was used for Western blot analysis. Nonimmune mouse IgG and HRP-coupled secondary antibodies were purchased from Sigma-Aldrich. Secondary antibodies conjugated with Alexa fluorophore 488, 555, or 647 were purchased from Invitrogen. Acti-stain 670 fluorescent phalloidin (PHDN1-A; Cytoskeleton) was used for F-actin staining. Alexa Fluor 594–conjugated DNase I (D12372; Molecular Probes) was used for G-actin staining.

Mice

Homozygous NCAM-floxed mice (NCAMff$^{+/+}$; Bukalo et al., 2004) were crossed with Nestin-cre transgenic mice (003771; The Jackson Laboratory) to generate conditionally NCAM-deficient (NCAMff$^{+/+}$cre$^{+/-}$, NCAM-cKO) mice and their control littermates (referred to as NCAMff$^{+/+}$cre$^{-/-}$ or NCAMff$^{+/-}$cre$^{-/-}$). Successful mating was verified by the presence of a vaginal plug. Observation date of the plug was considered E0.5. Mice had been backcrossed with C57BL/6J mice for >10 generations and were maintained on the C57BL/6J background thereafter. All experimental procedures were in accordance with Animal Research: Reporting of In Vivo Experiments guidelines and were approved by the institutional animal care and use committee of Soochow University.

DNA constructs, protein expression, and ELISA

Sequences of the intracellular domain of rat NCAM140 (NCAM140ICD) and NCAM180 (NCAM180ICD) were subcloned from prokaryotic expression pQE30-NCAM140ICD and pQE30-NCAM180ICD plasmids (Li et al., 2013) into pET29b-His vector (69872; Novagen). pET29b-NCAM140ICD was used as a template to produce the mutant NCAM140ICD expression vector, pET29b-muNCAM140ICD, by site-directed mutagenesis with CTG

encoding L^{749} mutated into GCG and TGT encoding C^{750} mutated into TCT. Primers for mutagenesis were 5′-TGCATCGCTGTTAAC GCGTCTGGCAAAGCTGGG-3′ (forward) and 5′-CATGAGCAGGCC ACACTTGTTCAGGAAGTAGCAGG-3′ (reverse). pET29b-profilin2 was synthesized by Takara Biotechnology. The profilin2 sequence was subcloned into a pCDH-EF1-MCS-T2A-copGFP vector. The pEX4-siRNA–resistant profilin2 plasmid was generated by GenePharma using pEX4-profilin2 as a template for three synonymous mutations on the siProfilin2 recognition sequence with 5′-CAT CACGCCAGTAGAAATA-3′ mutated into 5′-CATTACTCCAGTTGA AATA-3′. All plasmid constructs were verified by sequencing. Prokaryotic pET29b-NCAM140ICD, pET29b-muNCAM140ICD, pET29b-NCAM180ICD, and pET29b-profilin2 plasmids were transformed and expressed in *Escherichia coli* strain BL21, and corresponding recombinant proteins were purified by Ni-nitrilotriacetic acid chromatography (30210; Qiagen).

Profilin2 (100 µg/ml) was immobilized overnight at 4°C on a polyvinylchloride surface in 96-well ELISA plates (2595; Corning). Then, the wells were washed three times with PBS with 0.1% Tween 20 (PBST; pH 7.4) and blocked with 3% BSA in carbonate buffer (35 mM $NaHCO_3$ and 15 mM Na_2CO_3, pH 9.6) at 37°C for 2 h. Thereafter, increasing concentrations (0.1–12.5 µM) of recombinant NCAM140ICD, NCAM180ICD, or muNCAM140ICD (in PBST) were applied at 37°C for 2 h. After three washes, the wells were incubated with NCAM monoclonal antibodies (0.5 µg/ml) for 1.5 h at 37°C. Following five washes with PBST, HRP-conjugated secondary antibodies were applied for 1 h at 37°C. After five washes, protein binding was analyzed by adding the HRP substrate, tetramethylbenzidine reagent (34021; Thermo Fisher Scientific). The reaction was terminated with 2 M H_2SO_4, and ODs were measured at 450 nm using a plate reader (51119000; Thermo Fisher Scientific). Biotinylated peptides comprising aa sequences 729–750, 748–763, 756–770, 764–777, and 766–810 of mouse NCAM140; ^{745}IAV NLC GKA^{753} peptide comprising the profilin2 binding site; and mutated ^{745}IAV NAS GKA^{753} and ^{745}IAV QAC GKA^{753} peptides were synthesized by SciLight-Peptide Biotechnology. All constructs were incubated with substrate-coated profilin2 and detected by HRP-coupled NeutrAvidin (31030; Thermo Fisher Scientific).

RNAi

siProfilin2-399 (5′-CAUCACGCCAGUAGAAAUATT-3′), siProfilin2-527 (5′-CAAUGGACAUCCGGACAAATT), siNCAM (5′-GUUGGA GAGUCCAAAUUCUTT-3′), and NC (5′-UUCUCCGAACGUGUCACG UTT-3′) were synthesized by GenePharma. shProfilin2 was constructed by GeneChem by inserting the same target sequence as siProfilin2-399 into the GV102 vector. To confirm siProfilin2 efficacy, Neuro-2a cells (ATCC CCL-131; American Type Culture Collection) were transfected with siRNA/shRNA using Lipofectamine 2000 reagent according to the manufacturer's instructions (11668030; Invitrogen). MEFs (ATCC SCRC-1008; American Type Culture Collection) were transfected with siRNA using Lipofectamine 2000. The profilin2/NCAM knockdown efficacy was verified by Western blot analysis of cell lysates. Cultured NPCs were transfected with 20 pmol of RNA per cuvette using the Amaxa Nucleofector system (VPG-1004; Lonza) according to the user's manual.

Culture and transfection of NPCs

NPCs were obtained from the telencephalic lateral ventricle walls of E14 embryos and cultured in Gibco DMEM/F-12 culture medium (11320033; Thermo Fisher Scientific) supplemented with 2% Gibco B-27 (17504044; Thermo Fisher Scientific), 20 ng/ml bFGF (96-450-33; PeproTech), and 20 ng/ml EGF (315-09; PeproTech) as described previously (Ma et al., 2008). For differentiation, NPCs were cultured in DMEM/F-12 medium containing 2% B-27 and 0.5% Gibco FCS (Thermo Fisher Scientific) without EGF and bFGF for 5–7 d.

For NCAM antibody incubation experiments, NCAM antibodies (10 µg/ml) were added to the culture medium and replenished every 24 h. The medium was changed every 48 h.

Transfection of cultured NPCs was performed using the Amaxa Nucleofector system (VPG-1004; Lonza) according to the user's manual.

Lentiviral transduction

Lentivirus constructs containing full-length wild-type or mutated mouse NCAM140 genes were generated by GeneChem in an Ubi-MCS-3FLAG-SV40-EGFP-IRES-puromycin (GV358) vector comprising ubiquitin, SV40, and cytomegalovirus promoters. Cultured NPCs and MEFs were transduced with 10^8 transduction units/ml lentivirus following the manufacturer's instructions and thereafter maintained for 2–4 d.

BrdU labeling

For analysis of proliferation in vivo, pregnant mice were intraperitoneally injected with BrdU (50 mg/kg; B5002; Sigma-Aldrich) at different embryonic stages (E12, E14, E16, and E18) and sacrificed 30 min thereafter (Wu et al., 2017). For determination of the cell cycle exit, BrdU (100 mg/kg) was intraperitoneally injected into pregnant mice, and mice were sacrificed 18 h after injection. The cell cycle exit index was calculated as $BrdU^+Ki67^-$/total $BrdU^+$ cells (the percentage of cells exiting the cell cycle). The length of S-phase of the cell cycle was calculated as $BrdU^+Ki67^+$/total $Ki67^+$ cells.

For pulse-chase labeling of newborn cells, pregnant mice were intraperitoneally injected with BrdU (100 mg/kg) at E11.5, E14.5, and E15.5 and sacrificed at E18 or injected with BrdU at E16.5 and sacrificed at P2. Quantification of birth-dated neurons was performed by calculating the percentages of $BrdU^+$ layer-specific neuronal $marker^+$ cells/total layer-specific neuronal $marker^+$ ($Tbr1^+$, $Ctip2^+$, or $Cux1^+$) cells. Quantitation of birth-dated oligodendrocytes was performed by calculating the percentage of $Olig2^+BrdU^+$ cells/total $Olig2^+$ cells. Quantification of birth-dated astrocytes was calculated as the number of $GFAP^+BrdU^+$ cells along the dorsolateral VZ.

To investigate NPC proliferation in vitro, cells were cultured for 4–5 h in NPC culture medium supplemented with 10 µM BrdU.

Immunohistochemistry and image analysis

Immunohistochemistry was performed as described elsewhere (Wu et al., 2017). Briefly, pregnant mice were sacrificed, and the fetuses were removed from the uterus. Fetal brains were fixed in 4% formaldehyde in PBS (pH 7.3) for 24 h at 4°C followed by

sequential dehydration using 15% and 30% sucrose in PBS. Coronal sections (14 µm thick) were sectioned with a cryostat (CM1950; Leica Biosystems) and washed three times with PBS before being blocked in 10% donkey serum in 0.1% Triton X-100 in PBS for 1 h at room temperature. Primary antibodies were applied in the blocking solution for 16 h at 4°C, followed by three washes in PBS. Secondary antibodies were incubated in the blocking solution for 1 h at room temperature. Sections were then washed, air dried, and mounted using DAPI Fluoromount-G (0100-20; SouthernBiotech). Fluorescence images were acquired with an Axio Scope.A1 microscope (20× lens objective, ZEN 2.6 acquisition software [blue edition]; Carl Zeiss Microscopy) or an LSM700 confocal laser-scanning microscope (20×, 40×, 40× oil, or 63× oil lens objective, ZEN acquisition software version 2011; Carl Zeiss Microscopy) at room temperature. NCAM and profilin2 immunofluorescence intensity was quantified by ImageJ. Identical telencephalon cortical regions from littermates of control and NCAM-cKO mice (five sections per brain) were analyzed. NCAM/profilin2 immunofluorescence intensity was calculated as NCAM/profilin2 immunofluorescence intensity in different cortical regions in relation to the whole dorsal cortices. The average fluorescence density of NCAM/profilin2 was obtained by calculating the fluorescence density within a 250-µm^2 area in different cortical layers. Cortical cells were counted in regions as described previously (Cappello et al., 2006; Seuntjens et al., 2009). In brief, Tbr1$^+$ and ctip2$^+$ cells were counted in the medial brain because they distribute evenly in layers VI and V of the dorsal cortex; Cux1$^+$ and Olig2$^+$ cells in the lateral brain regions, where they appear first; and GFAP$^+$ cells in the dorsal pallium adjacent to the VZ, where they reside. The total GFAP$^+$ intensity was counted in VZ/SVZ because there are few GFAP$^+$ cells appearing in the wild type at E16 and the earlier appearing GFAP$^+$ cells do not distribute evenly in the VZ/SVZ (Fig. S5). Proliferating (i.e., BrdU$^+$, Ki67$^+$, and PH3$^+$), Tbr2$^+$, Pax6$^+$, Tbr1$^+$, and Ctip2$^+$ cells were counted in 100 × 250-µm areas in the dorsal pallium perpendicular to the VZ (Fig. S5, red rectangle), and numbers of Cux1$^+$ and Olig2$^+$ cells were counted in 100 × 250-µm areas of the dorsolateral pallium (blue rectangle). Numbers of caspase3$^+$ cells were determined in the entire hemitelencephalon cortex. The GFAP expression per unit area (150 × 150-µm) was measured in the dorsolateral pallium adjacent to VZ using ImageJ (Fig. S5, purple square).

For cortical neuron distribution analysis, the maximum migration of neonatal cortical neurons was measured as the vertical distance from VZ to the destination of different layers using ImageJ. The length of the entire cortical layers perpendicular to the VZ was measured using ImageJ and defined as total cortical length. The distribution of layer-specific marker$^+$ (Tbr1$^+$, Ctip2$^+$, or Cux1$^+$) neurons was quantified by calculating maximum migration distance of each type of neuron/total cortical length (shown by schematic diagram in Fig. S3).

Yeast two-hybrid screening

Yeast two-hybrid screening was performed with the ProQuest Two-Hybrid System (10835; Invitrogen) in *Saccharomyces cerevisiae* strain MaV203 following the manufacturer's protocol. The DNA fragment encoding the intracellular domain of mouse NCAM140 was used as bait.

Coimmunoprecipitation

Lysates of brains from newborn C57BL/6J mice were prepared using ice-cold lysis buffer (10 mM Tris-HCl, pH 7.5, 150 mM NaCl, 0.5% Triton X-100, 1% sodium deoxycholate, 0.5% SDS, 2 mM EDTA, and protease inhibitor cocktail [11697498001; Roche]). Lysates were centrifuged for 10 min at 15,000 *g* and 4°C, cleared with protein A/G-agarose beads (sc-2003, RRID: AB_10201400; Santa Cruz Biotechnology), and incubated with corresponding antibodies or, for negative control, nonimmune IgG at 4°C overnight. Antibody–protein complexes were collected by incubating lysates with protein A/G-agarose beads for 3 h at 4°C, pelleting the beads, and washing in PBS. Proteins were eluted with 2× SDS sample buffer by boiling the beads for 10 min and then subjected to Western blot analysis.

Quantitative real-time PCR

Total RNA was extracted from cultured NPCs using TRIzol reagent (15596018; Invitrogen). Reverse transcription reactions were performed with the EasyScript One-Step gDNA Removal and cDNA Synthesis SuperMix kits (AE311-02; Transgen Biotech). PCR primers were: forward 5′-GCCTATACGTTGATGGTG ACTG-3′, reverse 5′-ACAAAGACCAAGACTCTCCCG-3′ for profilin2, forward 5′-GACAGAACCCGAAAAGGGC-3′, reverse 5′-GTTGGGGACCGTCTTGACTT-3′ for NCAM, forward 5′-AGGTCG GTGTGAACGGATTTG-3′, reverse 5′-TGTAGACCATGTAGTTGA GGTCA-3′ for GAPDH. The reaction procedure was conducted at 94°C, 15 min (1 cycle); 95°C, 30 s; 55°C, 30 s; 72°C, 60 s (30 cycles), and 72°C, 8 min (1 cycle).

Immunocytochemistry and image analysis

Immunocytochemistry was performed as described elsewhere (Ma et al., 2008). Briefly, cells were fixed in 4% PFA in PBS for 15 min, permeabilized by 0.1% Triton X-100 in PBS for 5 min, and blocked by 10% donkey serum in 0.1% Triton X-100 in PBS for 1 h at room temperature. Cells were incubated with appropriate dilutions of primary antibodies in the blocking solution at 4°C overnight. Cells were then rinsed with PBS and incubated with corresponding secondary antibodies in the blocking solution for 1 h at room temperature. The culture was rinsed three times with PBS and counterstained with DAPI Fluoromount-G (0100-20; SouthernBiotech). To detect BrdU in cultured NPCs, cells were treated with 2 N HCl for 10 min at 37°C. The proportion of proliferating NPCs was quantified as the number of BrdU$^+$ cells divided by the total number of DAPI$^+$ cells. To estimate differentiation into neurons, astrocytes, and oligodendrocytes, numbers of Tuj1$^+$, GFAP$^+$, or O4$^+$ cells, respectively, were divided by the total number of DAPI$^+$ cells. Proliferation and differentiation of siProfilin2-transfected NPCs were quantified from random images of areas containing cultured cells. The proportion of target cells was quantified as the numbers of BrdU$^+$, Tuj1$^+$, GFAP$^+$, or O4$^+$ cells divided by the total number of DAPI$^+$ cells in the same field. Proliferation and differentiation of NPCs transfected with plasmids encoding profilin2, NCAM, and mutNCAM were quantified from images of areas captured

from top to bottom and left to right across the entire coverslip. The proportion of target cells was quantified as the numbers of $BrdU^+GFP^+$, $Tuj1^+GFP^+$, and $GFAP^+GFP^+$ cells divided by the total number of GFP^+ cells in the same coverslip. Each experiment was performed in independent triplicates.

F- and G-actin analysis

F- and G-actin levels were analyzed by Western blotting using an F-actin/G-actin in vivo assay kit (BK037; Cytoskeleton). Briefly, cultured NPCs were lysed with prewarmed F-actin stabilization buffer (50 mM Pipes buffer, pH 6.9, 50 mM NaCl, 5 mM $MgCl_2$, 5 mM EGTA, 5% [vol/vol] glycerol, 0.1% NP-40, 0.1% Triton X-100, 0.1% Tween 20, and 0.1% β-mercaptoethanol) at 37°C for 10 min. Samples were centrifuged at 100,000 *g* for 1 h at 37°C. Supernatants containing G-actin were separated from the pellets containing F-actin and placed on ice. The pellets were resuspended in the same volume as the supernatants using ice-cold water containing 1 µM cytochalasin D and incubated on ice for 1 h by pipetting up and down every 15 min to dissociate F-actin. Equal amounts of protein from each sample were subjected to Western blot analysis with anti-actin antibody with γ-tubulin serving as a control.

To analyze levels of G- and F-actin by microscopy, NPCs were costained by phalloidin (for F-actin) and DNase I (for G-actin). GFP-positive cells were outlined; the F- and G-actin labeling intensities were measured by Image Pro-plus 6.4 software (Media Cybernetics); and the ratio of F-actin/G-actin was calculated.

CSI analysis

The CSI analysis was performed as described elsewhere (Thakar et al., 2009). The coronal cortical sections at E12 were immunostained for actin with DAPI counterstaining to visualize cells and chromatin. Mitotic NPCs at metaphase and anaphase were identified by chromosome morphology at the VZ surface, selected, and analyzed (Haydar et al., 2003; Luxenburg et al., 2011). Cell boundaries were outlined with ImageJ. Cell area and perimeter were determined, and the CSI was calculated as follows: $CSI = 4\pi \times area/(perimeter)^2$. The CSI assumes values between 1 (circular shape) and 0 (elongated, linear morphology; Thakar et al., 2009).

Statistical analysis

Data were collected from at least three independent experiments ($n \geq 3$) or at least three pairs of NCAM-cKO mice and control littermates ($n \geq 3$; five slices from each animal). Values are presented as mean ± SEM. Data distribution was checked by Kolmogorov-Smirnov test. Statistical difference was tested by Student's *t* test, one-way ANOVA, or two-way ANOVA (for normally distributed data), and Mann-Whitney or Kruskal-Wallis test (for nonnormally distributed data) with appropriate post hoc analysis using SPSS Statistics 22.0 software (IBM; all two-sided). $P < 0.05$ was considered statistically significant (*, $P < 0.05$; **, $P < 0.01$; and ***, $P < 0.001$).

Online supplemental material

Fig. S1 shows the expression of NCAM and profilin2 in the developing cerebral cortex. Fig. S2 demonstrates that NCAM deficiency does not lead to increased NPC apoptosis during embryonic development. Fig. S3 shows that NCAM deficiency does not affect the distribution of neonatal cortical neurons in the coronal plane. Fig. S4 demonstrates that profilin2 expression is downregulated specifically by profilin2 RNAi. Fig. S5 displays a schematic diagram showing areas chosen for quantification of cells in imaging analysis.

Acknowledgments

This work was supported by the National Natural Science Foundation of China (81300985, 81870897, 81671111, and 81601111), the Natural Science Foundation of Liaoning Province (2019-MS-075), the Liaoning Revitalization Talents Program (XLYC1807124), the Dalian Technology Innovation Program (2019J13SN109), the Natural Science Foundation of Jiangsu Province (BK20181436), the Guangdong Key Project in "Development of new tools for diagnosis and treatment of autism" (2018B030335001), the Priority Academic Program Development of Jiangsu Higher Education Institution (PAPD), the Suzhou Clinical Research Center of Neurological Disease (Szzx201503), the Jiangsu Provincial Medical Key Discipline Project (ZDXKB2016022), the Jiangsu Provincial Special Program of Medical Science (BL2014042), the Jiangsu Key Laboratory of Translational Research and Therapy for Neuro-Psycho-Diseases (BM2013003), the Health Commission of Dalian (1711014), and the Li Ka Shing Foundation.

The authors declare no competing financial interests.

Author contributions: M. Schachner, V. Sytnyk, J. Boltze, Q.-H. Ma, and S. Li conceived and designed the experiments. R. Huang, D.-J. Yuan, S. Li, X.-S. Liang, Y. Gao, X.-Y. Lan, H.-M. Qin, and G.-Y. Xu performed the experiments and analyzed the data. R. Huang, Y.-F. Ma, V. Sytnyk, M. Schachner, J. Boltze, H.-M. Qin, Q.-H. Ma, and S. Li wrote the paper.

Submitted: 26 February 2019
Revised: 31 August 2019
Accepted: 21 October 2019

References

Amoureux, M.C., B.A. Cunningham, G.M. Edelman, and K.L. Crossin. 2000. N-CAM binding inhibits the proliferation of hippocampal progenitor cells and promotes their differentiation to a neuronal phenotype. *J. Neurosci.* 20:3631–3640. https://doi.org/10.1523/JNEUROSCI.20-10-03631.2000

Angata, K., V. Huckaby, B. Ranscht, A. Terskikh, J.D. Marth, and M. Fukuda. 2007. Polysialic acid-directed migration and differentiation of neural precursors are essential for mouse brain development. *Mol. Cell. Biol.* 27: 6659–6668. https://doi.org/10.1128/MCB.00205-07

Baracskay, K.L., G.J. Kidd, R.H. Miller, and B.D. Trapp. 2007. NG2-positive cells generate A2B5-positive oligodendrocyte precursor cells. *Glia.* 55: 1001–1010. https://doi.org/10.1002/glia.20519

Bonfanti, L. 2006. PSA-NCAM in mammalian structural plasticity and neurogenesis. *Prog. Neurobiol.* 80:129–164. https://doi.org/10.1016/j.pneurobio.2006.08.003

Boutin, C., B. Schmitz, H. Cremer, and S. Diestel. 2009. NCAM expression induces neurogenesis in vivo. *Eur. J. Neurosci.* 30:1209–1218. https://doi.org/10.1111/j.1460-9568.2009.06928.x

Brandewiede, J., O. Stork, and M. Schachner. 2014. NCAM deficiency in the mouse forebrain impairs innate and learned avoidance behaviours. *Genes Brain Behav.* 13:468–477. https://doi.org/10.1111/gbb.12138

Brennaman, L.H., and P.F. Maness. 2010. NCAM in neuropsychiatric and neurodegenerative disorders. *Adv. Exp. Med. Biol.* 663:299–317. https://doi.org/10.1007/978-1-4419-1170-4_19

Bukalo, O., N. Fentrop, A.Y. Lee, B. Salmen, J.W. Law, C.T. Wotjak, M. Schweizer, A. Dityatev, and M. Schachner. 2004. Conditional ablation of the neural cell adhesion molecule reduces precision of spatial learning, long-term potentiation, and depression in the CA1 subfield of mouse hippocampus. *J. Neurosci.* 24:1565–1577. https://doi.org/10.1523/JNEUROSCI.3298-03.2004

Burgess, A., S.R. Wainwright, L.S. Shihabuddin, U. Rutishauser, T. Seki, and I. Aubert. 2008. Polysialic acid regulates the clustering, migration, and neuronal differentiation of progenitor cells in the adult hippocampus. *Dev. Neurobiol.* 68:1580–1590. https://doi.org/10.1002/dneu.20681

Cappello, S., A. Attardo, X. Wu, T. Iwasato, S. Itohara, M. Wilsch-Bräuninger, H.M. Eilken, M.A. Rieger, T.T. Schroeder, W.B. Huttner, et al. 2006. The Rho-GTPase cdc42 regulates neural progenitor fate at the apical surface. *Nat. Neurosci.* 9:1099–1107. https://doi.org/10.1038/nn1744

Chakraborty, J., M. Pandey, A.K. Navneet, T.A. Appukuttan, M. Varghese, S.C. Sreetama, U. Rajamma, and K.P. Mohanakumar. 2014. Profilin-2 increased expression and its altered interaction with β-actin in the striatum of 3-nitropropionic acid-induced Huntington's disease in rats. *Neuroscience.* 281:216–228. https://doi.org/10.1016/j.neuroscience.2014.09.035

Cremer, H., R. Lange, A. Christoph, M. Plomann, G. Vopper, J. Roes, R. Brown, S. Baldwin, P. Kraemer, S. Scheff, et al. 1994. Inactivation of the N-CAM gene in mice results in size reduction of the olfactory bulb and deficits in spatial learning [letter]. *Nature.* 367:455–459. https://doi.org/10.1038/367455a0

Cremisi, F., A. Philpott, and S. Ohnuma. 2003. Cell cycle and cell fate interactions in neural development. *Curr. Opin. Neurobiol.* 13:26–33. https://doi.org/10.1016/S0959-4388(03)00005-9

Da Silva, J.S., M. Medina, C. Zuliani, A. Di Nardo, W. Witke, and C.G. Dotti. 2003. RhoA/ROCK regulation of neuritogenesis via profilin IIa-mediated control of actin stability. *J. Cell Biol.* 162:1267–1279. https://doi.org/10.1083/jcb.200304021

Dehay, C., and H. Kennedy. 2007. Cell-cycle control and cortical development. *Nat. Rev. Neurosci.* 8:438–450. https://doi.org/10.1038/nrn2097

Di Nardo, A., R. Gareus, D. Kwiatkowski, and W. Witke. 2000. Alternative splicing of the mouse profilin II gene generates functionally different profilin isoforms. *J. Cell Sci.* 113:3795–3803.

Dietrich, J., M. Noble, and M. Mayer-Proschel. 2002. Characterization of A2B5$^+$ glial precursor cells from cryopreserved human fetal brain progenitor cells. *Glia.* 40:65–77. https://doi.org/10.1002/glia.10116

Feng, L., M.E. Hatten, and N. Heintz. 1994. Brain lipid-binding protein (BLBP): a novel signaling system in the developing mammalian CNS. *Neuron.* 12:895–908. https://doi.org/10.1016/0896-6273(94)90341-7

Gal, J.S., Y.M. Morozov, A.E. Ayoub, M. Chatterjee, P. Rakic, and T.F. Haydar. 2006. Molecular and morphological heterogeneity of neural precursors in the mouse neocortical proliferative zones. *J. Neurosci.* 26:1045–1056. https://doi.org/10.1523/JNEUROSCI.4499-05.2006

Gaspard, N., and P. Vanderhaeghen. 2011. From stem cells to neural networks: recent advances and perspectives for neurodevelopmental disorders. *Dev. Med. Child Neurol.* 53:13–17. https://doi.org/10.1111/j.1469-8749.2010.03827.x

Greig, L.C., M.B. Woodworth, M.J. Galazo, H. Padmanabhan, and J.D. Macklis. 2013. Molecular logic of neocortical projection neuron specification, development and diversity. *Nat. Rev. Neurosci.* 14:755–769. https://doi.org/10.1038/nrn3586

Haubensak, W., A. Attardo, W. Denk, and W.B. Huttner. 2004. Neurons arise in the basal neuroepithelium of the early mammalian telencephalon: a major site of neurogenesis. *Proc. Natl. Acad. Sci. USA.* 101:3196–3201. https://doi.org/10.1073/pnas.0308600100

Haydar, T.F., E. Ang Jr., and P. Rakic. 2003. Mitotic spindle rotation and mode of cell division in the developing telencephalon. *Proc. Natl. Acad. Sci. USA.* 100:2890–2895. https://doi.org/10.1073/pnas.0437969100

Hegedus, B., B. Dasgupta, J.E. Shin, R.J. Emnett, E.K. Hart-Mahon, L. Elghazi, E. Bernal-Mizrachi, and D.H. Gutmann. 2007. Neurofibromatosis-1 regulates neuronal and glial cell differentiation from neuroglial progenitors in vivo by both cAMP- and Ras-dependent mechanisms. *Cell Stem Cell.* 1:443–457. https://doi.org/10.1016/j.stem.2007.07.008

Heng, Y.W., and C.G. Koh. 2010. Actin cytoskeleton dynamics and the cell division cycle. *Int. J. Biochem. Cell Biol.* 42:1622–1633. https://doi.org/10.1016/j.biocel.2010.04.007

Hidese, S., K. Hattori, D. Sasayama, T. Miyakawa, R. Matsumura, Y. Yokota, I. Ishida, J. Matsuo, T. Noda, S. Yoshida, et al. 2017. Cerebrospinal fluid neural cell adhesion molecule levels and their correlation with clinical variables in patients with schizophrenia, bipolar disorder, and major depressive disorder. *Prog. Neuropsychopharmacol. Biol. Psychiatry.* 76:12–18. https://doi.org/10.1016/j.pnpbp.2017.02.016

Hübschmann, M.V., G. Skladchikova, E. Bock, and V. Berezin. 2005. Neural cell adhesion molecule function is regulated by metalloproteinase-mediated ectodomain release. *J. Neurosci. Res.* 80:826–837. https://doi.org/10.1002/jnr.20530

Jacobs, S., and L.C. Doering. 2010. Astrocytes prevent abnormal neuronal development in the fragile X mouse. *J. Neurosci.* 30:4508–4514. https://doi.org/10.1523/JNEUROSCI.5027-09.2010

Kim, B.W., and H. Son. 2006. Neural cell adhesion molecule (NCAM) induces neuronal phenotype acquisition in dominant negative MEK1-expressing hippocampal neural progenitor cells. *Exp. Mol. Med.* 38:732–738. https://doi.org/10.1038/emm.2006.86

Kim, J.H., J.H. Lee, J.Y. Park, C.H. Park, C.O. Yun, S.H. Lee, Y.S. Lee, and H. Son. 2005. Retrovirally transduced NCAM140 facilitates neuronal fate choice of hippocampal progenitor cells. *J. Neurochem.* 94:417–424. https://doi.org/10.1111/j.1471-4159.2005.03208.x

Klein, R., S. Blaschke, B. Neumaier, H. Endepols, R. Graf, M. Keuters, J. Hucklenbroich, M. Albrechtsen, S. Rees, G.R. Fink, et al. 2014. The synthetic NCAM mimetic peptide FGL mobilizes neural stem cells in vitro and in vivo. *Stem Cell Rev. Rep.* 10:539–547. https://doi.org/10.1007/s12015-014-9512-5

Kohl, C., O. Riccio, J. Grosse, O. Zanoletti, C. Fournier, S.M. Klampfl, M.V. Schmidt, and C. Sandi. 2013. The interplay of conditional NCAM-knockout and chronic unpredictable stress leads to increased aggression in mice. *Stress.* 16:647–654. https://doi.org/10.3109/10253890.2013.840824

Kohwi, M., and C.Q. Doe. 2013. Temporal fate specification and neural progenitor competence during development. *Nat. Rev. Neurosci.* 14:823–838. https://doi.org/10.1038/nrn3618

Korshunova, I., V. Novitskaya, D. Kiryushko, N. Pedersen, K. Kolkova, E. Kropotova, M. Mosevitsky, M. Rayko, J.S. Morrow, I. Ginzburg, et al. 2007. GAP-43 regulates NCAM-180-mediated neurite outgrowth. *J. Neurochem.* 100:1599–1612.

Kunda, P., and B. Baum. 2009. The actin cytoskeleton in spindle assembly and positioning. *Trends Cell Biol.* 19:174–179. https://doi.org/10.1016/j.tcb.2009.01.006

Kurtz, A., A. Zimmer, F. Schnütgen, G. Brüning, F. Spener, and T. Müller. 1994. The expression pattern of a novel gene encoding brain-fatty acid binding protein correlates with neuronal and glial cell development. *Development.* 120:2637–2649.

Lamprecht, R., C.R. Farb, S.M. Rodrigues, and J.E. LeDoux. 2006. Fear conditioning drives profilin into amygdala dendritic spines. *Nat. Neurosci.* 9:481–483. https://doi.org/10.1038/nn1672

Li, S., I. Leshchyns'ka, Y. Chernyshova, M. Schachner, and V. Sytnyk. 2013. The neural cell adhesion molecule (NCAM) associates with and signals through p21-activated kinase 1 (Pak1). *J. Neurosci.* 33:790–803. https://doi.org/10.1523/JNEUROSCI.1238-12.2013

Luxenburg, C., H.A. Pasolli, S.E. Williams, and E. Fuchs. 2011. Developmental roles for Srf, cortical cytoskeleton and cell shape in epidermal spindle orientation. *Nat. Cell Biol.* 13:203–214. https://doi.org/10.1038/ncb2163

Ma, Q.H., T. Futagawa, W.L. Yang, X.D. Jiang, L. Zeng, Y. Takeda, R.X. Xu, D. Bagnard, M. Schachner, A.J. Furley, et al. 2008. A TAG1-APP signalling pathway through Fe65 negatively modulates neurogenesis. *Nat. Cell Biol.* 10:283–294. https://doi.org/10.1038/ncb1690

Michaelsen, K., K. Murk, M. Zagrebelsky, A. Drexnjak, B.M. Jockusch, M. Rothkegel, and M. Korte. 2010. Fine-tuning of neuronal architecture requires two profilin isoforms. *Proc. Natl. Acad. Sci. USA.* 107:15780–15785. https://doi.org/10.1073/pnas.1004406107

Miller, F.D., and A.S. Gauthier. 2007. Timing is everything: making neurons versus glia in the developing cortex. *Neuron.* 54:357–369. https://doi.org/10.1016/j.neuron.2007.04.019

Miralles, F., and N. Visa. 2006. Actin in transcription and transcription regulation. *Curr. Opin. Cell Biol.* 18:261–266. https://doi.org/10.1016/j.ceb.2006.04.009

Molofsky, A.V., R. Krencik, E.M. Ullian, H.H. Tsai, B. Deneen, W.D. Richardson, B.A. Barres, and D.H. Rowitch. 2012. Astrocytes and disease: a neurodevelopmental perspective. *Genes Dev.* 26:891–907. https://doi.org/10.1101/gad.188326.112

Paquin, A., C. Hordo, D.R. Kaplan, and F.D. Miller. 2009. Costello syndrome H-Ras alleles regulate cortical development. *Dev. Biol.* 330:440–451. https://doi.org/10.1016/j.ydbio.2009.04.010

Pillai-Nair, N., A.K. Panicker, R.M. Rodriguiz, K.L. Gilmore, G.P. Demyanenko, J.Z. Huang, W.C. Wetsel, and P.F. Maness. 2005. Neural cell

adhesion molecule-secreting transgenic mice display abnormalities in GABAergic interneurons and alterations in behavior. *J. Neurosci.* 25: 4659–4671. https://doi.org/10.1523/JNEUROSCI.0565-05.2005

Pilo Boyl, P., A. Di Nardo, C. Mulle, M. Sassoè-Pognetto, P. Panzanelli, A. Mele, M. Kneussel, V. Costantini, E. Perlas, M. Massimi, et al. 2007. Profilin2 contributes to synaptic vesicle exocytosis, neuronal excitability, and novelty-seeking behavior. *EMBO J.* 26:2991–3002. https://doi.org/10.1038/sj.emboj.7601737

Politis, P.K., D. Thomaidou, and R. Matsas. 2008. Coordination of cell cycle exit and differentiation of neuronal progenitors. *Cell Cycle.* 7:691–697. https://doi.org/10.4161/cc.7.6.5550

Pollerberg, G.E., M. Schachner, and J. Davoust. 1986. Differentiation state-dependent surface mobilities of two forms of the neural cell adhesion molecule. *Nature.* 324:462–465. https://doi.org/10.1038/324462a0

Prodromidou, K., F. Papastefanaki, T. Sklaviadis, and R. Matsas. 2014. Functional cross-talk between the cellular prion protein and the neural cell adhesion molecule is critical for neuronal differentiation of neural stem/precursor cells. *Stem Cells.* 32:1674–1687. https://doi.org/10.1002/stem.1663

Puchkov, D., I. Leshchyns'ka, A.G. Nikonenko, M. Schachner, and V. Sytnyk. 2011. NCAM/spectrin complex disassembly results in PSD perforation and postsynaptic endocytic zone formation. *Cereb. Cortex.* 21:2217–2232. https://doi.org/10.1093/cercor/bhq283

Purcell, A.E., M.M. Rocco, J.A. Lenhart, K. Hyder, A.W. Zimmerman, and J. Pevsner. 2001. Assessment of neural cell adhesion molecule (NCAM) in autistic serum and postmortem brain. *J. Autism Dev. Disord.* 31:183–194. https://doi.org/10.1023/A:1010751232295

Schlüter, K., B.M. Jockusch, and M. Rothkegel. 1997. Profilins as regulators of actin dynamics. *Biochim. Biophys. Acta.* 1359:97–109. https://doi.org/10.1016/S0167-4889(97)00100-6

Secher, T. 2010. Soluble NCAM. *In* Structure and Function of the Neural Cell Adhesion Molecule NCAM. V. Berezin, editor. Springer, New York. 227–242. https://doi.org/10.1007/978-1-4419-1170-4_15

Seki, T., and Y. Arai. 1991. Expression of highly polysialylated NCAM in the neocortex and piriform cortex of the developing and the adult rat. *Anat. Embryol. (Berl.).* 184:395–401. https://doi.org/10.1007/BF00957900

Seuntjens, E., A. Nityanandam, A. Miquelajauregui, J. Debruyn, A. Stryjewska, S. Goebbels, K.A. Nave, D. Huylebroeck, and V. Tarabykin. 2009. Sip1 regulates sequential fate decisions by feedback signaling from postmitotic neurons to progenitors. *Nat. Neurosci.* 12:1373–1380. https://doi.org/10.1038/nn.2409

Shetty, A., V. Sytnyk, I. Leshchyns'ka, D. Puchkov, V. Haucke, and M. Schachner. 2013. The neural cell adhesion molecule promotes maturation of the presynaptic endocytotic machinery by switching synaptic vesicle recycling from adaptor protein 3 (AP-3)- to AP-2-dependent mechanisms. *J. Neurosci.* 33:16828–16845. https://doi.org/10.1523/JNEUROSCI.2192-13.2013

Shin, M.H., E.G. Lee, S.H. Lee, Y.S. Lee, and H. Son. 2002. Neural cell adhesion molecule (NCAM) promotes the differentiation of hippocampal precursor cells to a neuronal lineage, especially to a glutamatergic neural cell type. *Exp. Mol. Med.* 34:401–410. https://doi.org/10.1038/emm.2002.57

Sloan, S.A., and B.A. Barres. 2014. Mechanisms of astrocyte development and their contributions to neurodevelopmental disorders. *Curr. Opin. Neurobiol.* 27:75–81. https://doi.org/10.1016/j.conb.2014.03.005

Soroka, V., K. Kolkova, J.S. Kastrup, K. Diederichs, J. Breed, V.V. Kiselyov, F.M. Poulsen, I.K. Larsen, W. Welte, V. Berezin, et al. 2003. Structure and interactions of NCAM Ig1-2-3 suggest a novel zipper mechanism for homophilic adhesion. *Structure.* 11:1291–1301. https://doi.org/10.1016/j.str.2003.09.006

Stork, O., H. Welzl, H. Cremer, and M. Schachner. 1997. Increased intermale aggression and neuroendocrine response in mice deficient for the neural cell adhesion molecule (NCAM). *Eur. J. Neurosci.* 9:1117–1125. https://doi.org/10.1111/j.1460-9568.1997.tb01464.x

Stork, O., H. Welzl, C.T. Wotjak, D. Hoyer, M. Delling, H. Cremer, and M. Schachner. 1999. Anxiety and increased 5-HT1A receptor response in NCAM null mutant mice. *J. Neurobiol.* 40:343–355. https://doi.org/10.1002/(SICI)1097-4695(19990905)40:3<343::AID-NEU6>3.0.CO;2-S

Stork, O., H. Welzl, D. Wolfer, T. Schuster, N. Mantei, S. Stork, D. Hoyer, H. Lipp, K. Obata, and M. Schachner. 2000. Recovery of emotional behaviour in neural cell adhesion molecule (NCAM) null mutant mice through transgenic expression of NCAM180. *Eur. J. Neurosci.* 12: 3291–3306. https://doi.org/10.1046/j.1460-9568.2000.00197.x

Suetsugu, S., H. Miki, and T. Takenawa. 1999. Distinct roles of profilin in cell morphological changes: microspikes, membrane ruffles, stress fibers, and cytokinesis. *FEBS Lett.* 457:470–474. https://doi.org/10.1016/S0014-5793(99)01086-8

Sytnyk, V., I. Leshchyns'ka, A.G. Nikonenko, and M. Schachner. 2006. NCAM promotes assembly and activity-dependent remodeling of the postsynaptic signaling complex. *J. Cell Biol.* 174:1071–1085. https://doi.org/10.1083/jcb.200604145

Sytnyk, V., I. Leshchyns'ka, and M. Schachner. 2017. Neural cell adhesion molecules of the immunoglobulin superfamily regulate synapse formation, maintenance, and function. *Trends Neurosci.* 40:295–308. https://doi.org/10.1016/j.tins.2017.03.003

Tartaglia, M., E.L. Mehler, R. Goldberg, G. Zampino, H.G. Brunner, H. Kremer, I. van der Burgt, A.H. Crosby, A. Ion, S. Jeffery, et al. 2001. Mutations in PTPN11, encoding the protein tyrosine phosphatase SHP-2, cause Noonan syndrome. *Nat. Genet.* 29:465–468. https://doi.org/10.1038/ng772

Thakar, R.G., Q. Cheng, S. Patel, J. Chu, M. Nasir, D. Liepmann, K. Komvopoulos, and S. Li. 2009. Cell-shape regulation of smooth muscle cell proliferation. *Biophys. J.* 96:3423–3432. https://doi.org/10.1016/j.bpj.2008.11.074

Urosevic, J., V. Sauzeau, M.L. Soto-Montenegro, S. Reig, M. Desco, E.M. Wright, M. Cañamero, F. Mulero, S. Ortega, X.R. Bustelo, et al. 2011. Constitutive activation of B-Raf in the mouse germ line provides a model for human cardio-facio-cutaneous syndrome. *Proc. Natl. Acad. Sci. USA.* 108:5015–5020. https://doi.org/10.1073/pnas.1016933108

Vicente, A.M., F. Macciardi, M. Verga, A.S. Bassett, W.G. Honer, G. Bean, and J.L. Kennedy. 1997. NCAM and schizophrenia: genetic studies. *Mol. Psychiatry.* 2:65–69. https://doi.org/10.1038/sj.mp.4000235

Wang, D.D., and A. Bordey. 2008. The astrocyte odyssey. *Prog. Neurobiol.* 86: 342–367.

Wang, W., L. Wang, J. Luo, Z. Xi, X. Wang, G. Chen, and L. Chu. 2012. Role of a neural cell adhesion molecule found in cerebrospinal fluid as a potential biomarker for epilepsy. *Neurochem. Res.* 37:819–825. https://doi.org/10.1007/s11064-011-0677-x

Witke, W. 2004. The role of profilin complexes in cell motility and other cellular processes. *Trends Cell Biol.* 14:461–469. https://doi.org/10.1016/j.tcb.2004.07.003

Witke, W., A.V. Podtelejnikov, A. Di Nardo, J.D. Sutherland, C.B. Gurniak, C. Dotti, and M. Mann. 1998. In mouse brain profilin I and profilin II associate with regulators of the endocytic pathway and actin assembly. *EMBO J.* 17:967–976. https://doi.org/10.1093/emboj/17.4.967

Wood, G.K., H. Tomasiewicz, U. Rutishauser, T. Magnuson, R. Quirion, J. Rochford, and L.K. Srivastava. 1998. NCAM-180 knockout mice display increased lateral ventricle size and reduced prepulse inhibition of startle. *Neuroreport.* 9:461–466. https://doi.org/10.1097/00001756-199802160-00019

Wu, Z.Q., D. Li, Y. Huang, X.P. Chen, W. Huang, C.F. Liu, H.Q. Zhao, R.X. Xu, M. Cheng, M. Schachner, et al. 2017. Caspr controls the temporal specification of neural progenitor cells through Notch signaling in the developing mouse cerebral cortex. *Cereb. Cortex.* 27:1369–1385.

Zdaniuk, G., T. Wierzba-Bobrowicz, G.M. Szpak, and T. Stępień. 2011. Astroglia disturbances during development of the central nervous system in fetuses with Down's syndrome. *Folia Neuropathol.* 49:109–114.

Supplemental material

Huang et al., https://doi.org/10.1083/jcb.201902164

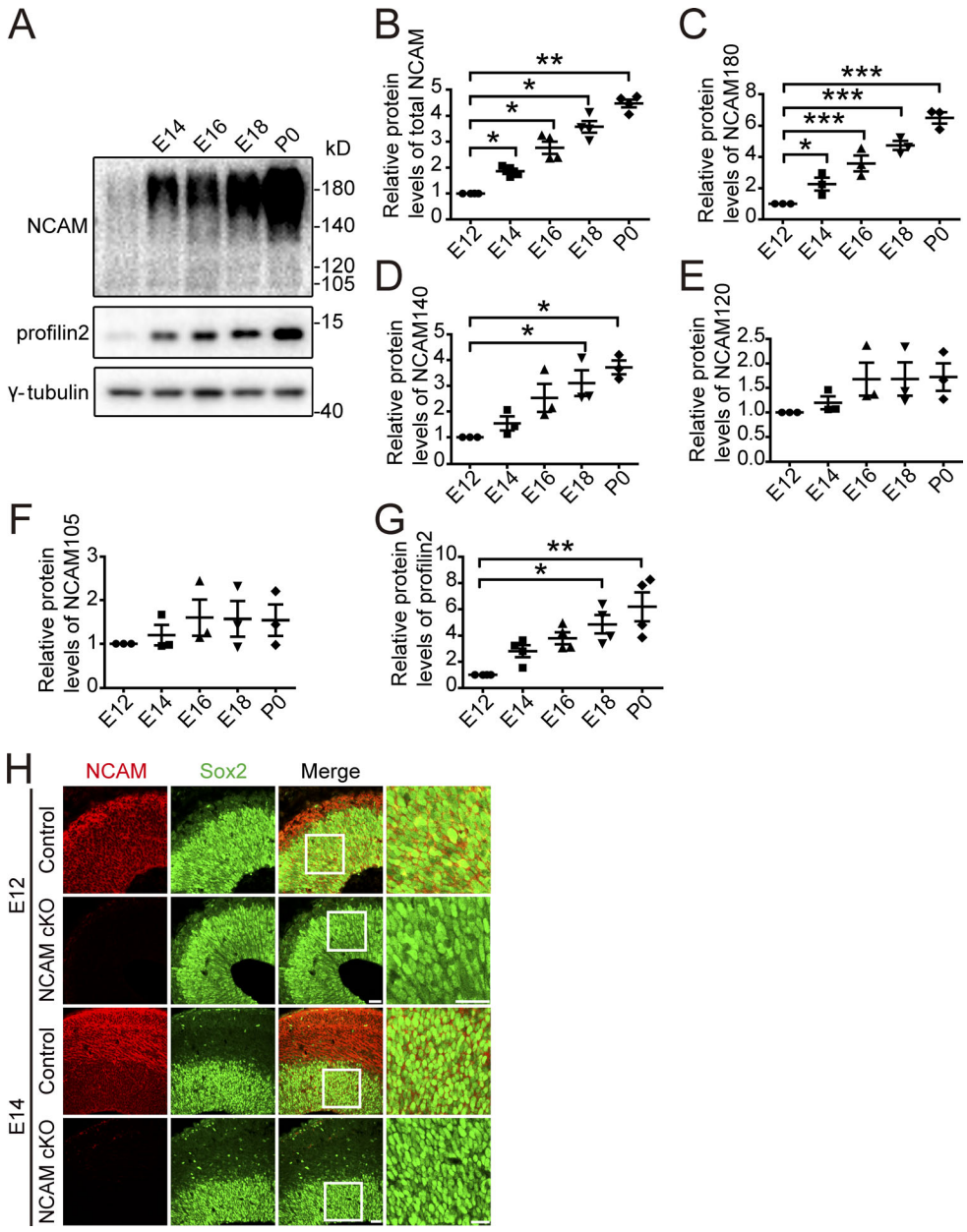

Figure S1. **Expression of NCAM and profilin2 in the developing cerebral cortex. (A–G)** Western blot analysis of NCAM and profilin2 expression in E12, E14, E16, E18, and P0 mouse cortices. γ-Tubulin served as a control. The protein levels in E14, E16, E18, and P0 mouse cortices were quantified relative to the protein levels in E12 mouse cortices set to 1.0. *n* = 3 or 4 biological replicates (total NCAM and profilin2, respectively). **(H)** Coronal sections of control and NCAM-cKO mouse cortices were coimmunostained for NCAM and Sox2 at E12 and E14. Scale bars, 20 µm. Values represent mean ± SEM. *, P < 0.05; **, P < 0.01; ***, P < 0.001 (two sided). One-way ANOVA with least significant difference correction (C and F), with Dunnett's T3 correction (B, D, and E), or Kruskal-Wallis test with Dunn-Bonferroni post hoc comparison (G).

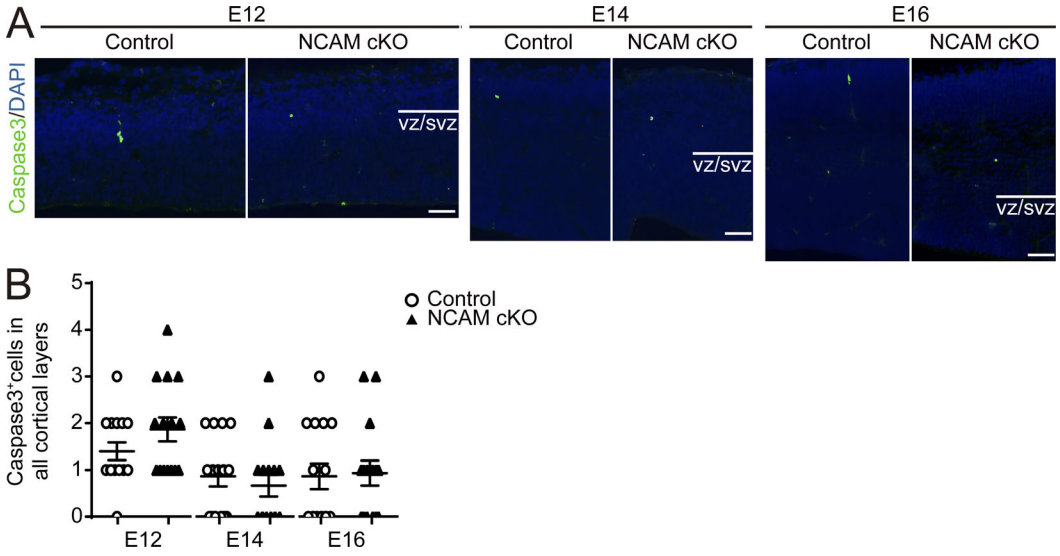

Figure S2. **NCAM deficiency does not lead to increased NPC apoptosis during embryonic development. (A)** Coronal sections of E12, E14, and E16 control and NCAM-cKO cortices were immunostained for activated, cleaved caspase3 and counterstained with DAPI. **(B)** Numbers of caspase3+ cells in the entire hemitelencephalon cortex. Mean ± SEM values. *n* = 15 brain slices from three mice. Mann-Whitney test did not reveal a statistically significant differences between groups. Scale bars, 50 µm.

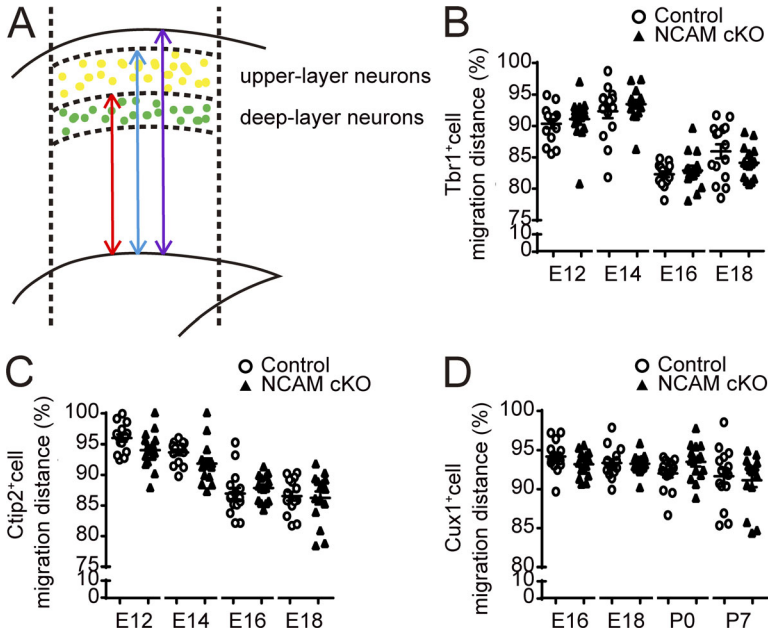

Figure S3. **NCAM deficiency does not affect the distribution of neonatal cortical neurons in the coronal plane. (A)** The cortical neuron distribution was analyzed by the maximum migration distance of deep-layer (red arrow) or upper-layer (blue arrow) neurons from VZ to cortical surface/total cortical length (purple arrow). **(B–D)** Percentages of the maximum migration distance of Tbr1+ (B), Ctip2+ (C), and Cux1+ (D) neurons in total cortical length. Mean ± SEM values. *n* = 15 brain slices from three mice. Student's *t* test or Mann-Whitney test (E12 and E14 in B and E18 in D).

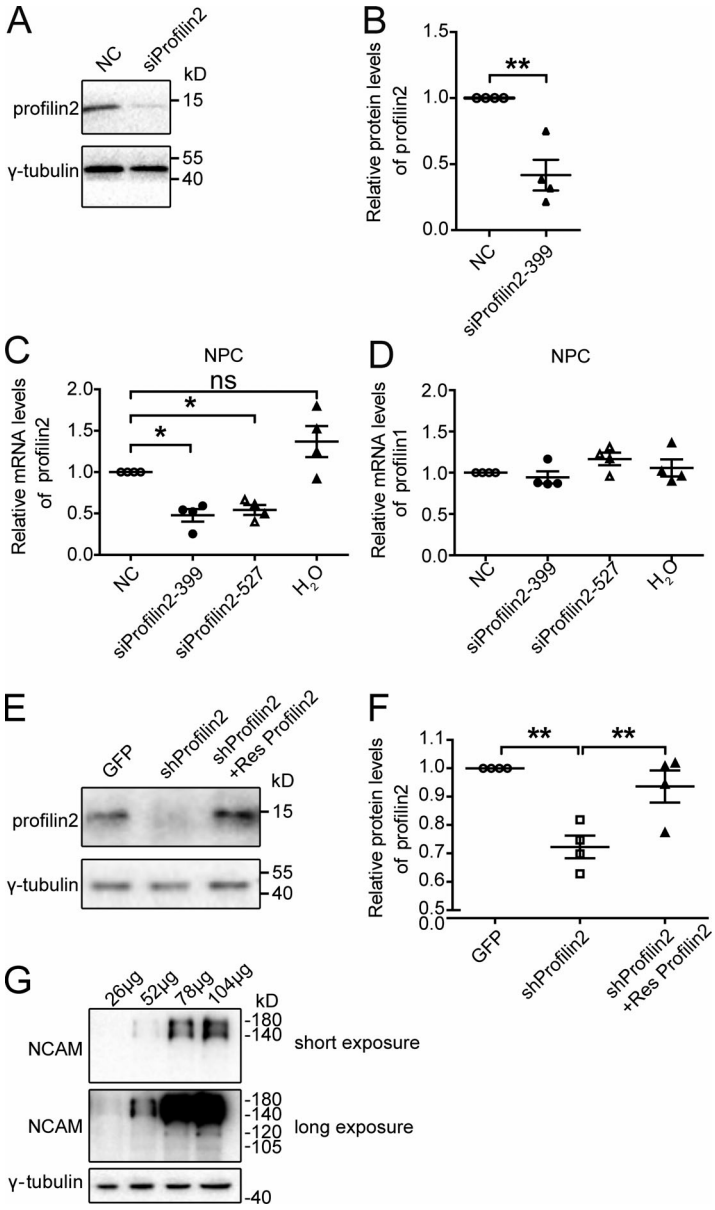

Figure S4. **Profilin2 expression is downregulated specifically by profilin2 RNAi. (A)** Western blot analysis of profilin2 levels in Neuro-2a cells transfected with either siProfilin2 or NC. **(B)** Levels of profilin2 in siProfilin2-transfected cells relative to those in NC-transfected cells, which were set to 1.0. **(C and D)** Quantitative PCR analysis of the levels of profilin2 (C) or profilin1 (D) mRNA in cultured NPCs transfected with either siProfilin2 (399 or 527) or NC. The mRNA levels of profilin2/1 in NC-transfected NPCs were set to 1.0. **(E and F)** Western blot analysis of profilin2 levels in Neuro-2a cells transfected with scrambled shRNA (GFP) or profilin2 shRNA (shProfilin2) only or cotransfected with shProfilin2 and shRNA-resistant profilin2 (Res Profilin2). The levels of profilin2 protein were quantified relative to those in GFP-transfected cells set to 1.0. **(G)** NCAM levels in brain homogenates loaded in different quantities (26, 53, 78, and 104 μg). Values represent mean ± SEM. *n* = 4 biological replicates. *, P < 0.05; **, P < 0.01 (two sided); ns, not statistically significant. Paired *t* test (B), one-way ANOVA with Dunnett's T3 correction (C and D), or least significant difference correction (F).

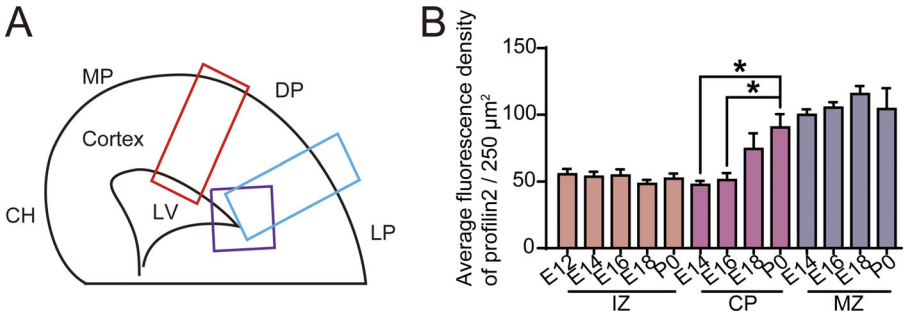

Figure S5. **Schematic diagram showing areas chosen for quantification of cells in imaging analysis. (A)** Red rectangle indicates the 100 × 250-µm area of interest in the dorsal pallium (DP) perpendicular to the VZ. Blue rectangle indicates the 100 × 250-µm areas of interest in the DP. Purple square indicates the 150 × 150-µm area of interest in the DP adjacent to VZ. CH, cortical hem; MP, medial pallium; LP, lateral pallium; LV, lateral ventricle (see Materials and methods for details). **(B)** Average immunofluorescence density of profilin2 in each cortical layer. *n* = 9 brain slices from three mice. Values represent mean ± SEM. *, P < 0.05 (two sided). Kruskal-Wallis test with Dunn-Bonferroni post hoc test (CP) and one-way ANOVA with Bonferroni correction (IZ and MZ).